NAV-0207-FM-95123-934

# IMIDE/GRAPHITE COMPOSITE DEGRADATION MECHANISM

M. Druy
J. Gassner
M. Groleau
R. Kovar
P. Wilson
Foster-Miller, Inc.
350 Second Avenue
Waltham, MA 02154-1196
(617) 290-0992



October 1995

Final Report
Contract No. N00019-94-C-0207
Contract Amount: $58,801.30
Contract Competitively Awarded

Prepared for

Naval Air Sytems Command (AIR-4.3.4)
Naval Air Systems Command Headquarters
1421 Jefferson Davis Highway
Arlington, VA 22243-5120
Attention: Mr. James Thompson

NAV-0207-FM-95123-934

# IMIDE/GRAPHITE COMPOSITE DEGRADATION MECHANISM

M. Druy
J. Gassner
M. Groleau
R. Kovar
P. Wilson
Foster-Miller, Inc.
350 Second Avenue
Waltham, MA 02154-1196
(617) 290-0992



October 1995

Final Report
Contract No. N00019-94-C-0207
Contract Amount: $58,801.30
Contract Competitively Awarded

Prepared for

Naval Air Sytems Command (AIR-4.3.4)
Naval Air Systems Command Headquarters
1421 Jefferson Davis Highway
Arlington, VA 22243-5120
Attention: Mr. James Thompson

*LICENSE RIGHTS LEGEND*
*Contract No. N00019-94-C-0207*
*Contractor or Subcontractor: Foster-Miller, Inc.*

*For a period of four (4) years after the delivery and acceptance of the last deliverable item under the above contract, this technical data shall be subject to the restrictions contained in the definition of "Limited Rights" in DFARS clause at 252.227-7013. After the four-year period, the data shall be subject to the restrictions contained in the definition of "Government Purpose License Rights" in DFARS clause 252.227-7013. The Government assumes no liability for unauthorized use or disclosure by others. This legend, together with the indications of the portions of the data which are subject to such limitations shall be included on any reproduction hereof which contains any portions subject to such limitations and shall be honored only as long as the data continues to meet the definition on Government purpose license rights.*

# REPORT DOCUMENTATION PAGE

*Form Approved*
*OMB No. 0704-0188*



| 1. AGENCY USE ONLY *(Leave blank)* | 2. REPORT DATE | 3. REPORT TYPE AND DATES COVERED |
|---|---|---|
| | October 1995 | Final Report 17 January 1995 - 31 July 1995 |

**4. TITLE AND SUBTITLE**

Imide/Graphite Composite Degradation Mechanism

**5. FUNDING NUMBERS**

N00019-93-P6-MP040

**6. AUTHOR(S)**

M. Druy, J. Gassner, M. Groleau, R. Kovar, P. Wilson

**7. PERFORMING ORGANIZATION NAME(S) AND ADDRESS(ES)**

Foster-Miller, Inc.
350 Second Avenue
Waltham, MA 02154-1196

**8. PERFORMING ORGANIZATION REPORT NUMBER**

NAV-0207-FM-95123-934

**9. SPONSORING/MONITORING AGENCY NAME(S) AND ADDRESS(ES)**

Naval Air Systems Command
Naval Air Systems Command Headquarters
1421 Jefferson Davis Highway
Arlington, VA 22243-5120

**10. SPONSORING/MONITORING AGENCY REPORT NUMBER**

N00019-94-C-0207

**11. SUPPLEMENTARY NOTES**

TPO: Mr. James Thompson, (AIR-4.3.4)

**12a. DISTRIBUTION/AVAILABILITY STATEMENT**

"Distribution approved for public release; distribution is unlimited. Disclosure outside the Government is subject to the restrictions of DFARS 227.405-79 (b)(1)."

**12b. DISTRIBUTION CODE**

N/A

**13. ABSTRACT** *(Maximum 200 words)*

This report presents the results of the Phase I research undertaken by Foster-Miller, Inc. to establish at the molecular level, the mechanism of degradation of composites employing bismaleimide (BMI) resins when in contact with a corroding metal in an electrolytic saltwater solution. It also discusses Foster-Miller's approach to reducing this degradation by modifying the resin with hydroxyl scavengers.

Our results indicated that samples which were modified with hydroxyl scavengers corroded at a rate greater than or equal to that of unmodified BMI control samples. Optical and SEM microscopy of corroded samples revealed that the main mechanism of corrosion was stress corrosion cracking. Microcracks first initiated in the surface resin, then propagated along the fiber-matrix interface beneath the resin surface, resulting in the peeling and flaking of large fragments of undegaded resin. In an effort to retard this mechanism, a sample containing epoxy-coated fibers was fabricated. It was postulated that the epoxy coating which is resistant to hydroxyl attack, might prevent the microcracks from propagating along the fiber matrix interface, thus preventing flaking of the resin. While the preliminary effort using epoxy coatings did not succeed in reducing corrosion, other polymeric coatings may be helpful in attaining this objective.

**14. SUBJECT TERM**

Bismaleimide degradation, stress-corrosion cracking, hydroxyl attack

**15. NUMBER OF PAGES**

49

**16. PRICE CODE**

N/A

| 17. SECURITY CLASSIFICATION OF REPORT | 18. SECURITY CLASSIFICATION OF THIS PAGE | 19. SECURITY CLASSIFICATION OF ABSTRACT | 20. LIMITATION OF ABSTRACT |
|---|---|---|---|
| Unclassified | Unclassified | Unclassified | Unlimited |

# CONTENTS

# ILLUSTRATIONS

**Figure** **Page**

# TABLES

# 1. SUMMARY

This report presents the results of the Phase I research undertaken by Foster-Miller, Inc. to establish, at the molecular level, the mechanism of degradation of composites employing bismaleimide (BMI) resins when in contact with a corroding metal in an electrolytic saltwater solution. It also discusses Foster-Miller's approach to reducing this corrosion by modifying the resin with hydroxyl scavengers. Imide-based composites form the principal family of thermosetting organic matrix materials having the ability to withstand operating temperatures greater that 300°F (1), and recent laboratory experiments have demonstrated that graphite fiber/imide based composites can degrade via a galvanic process that produces hydroxyl groups (2). The hydroxyl groups attack the imide ring in the matrix resin, producing amic acid salts and amines (3). The breakdown of the resin leads to resin loss in the plies of the composite and to degradation of the mechanical properties.

In the course of this research we:

- Determined the upper and lower bounds of the rate of corrosion for the unmodified BMI resin.
- Selected hydroxyl scavengers for modification of the BMI resin as a means for preventing corrosion.
- Fabricated composite test coupons.
- Corroded test coupons in a jet fuel - 3 percent saltwater mixture while attached to an aluminum post.
- Measured the bearing strength of corroded test coupons.
- Characterized test coupon corrosion via diffuse reflectance infrared (DRIFT) spectroscopy, optical microscopy, and SEM microscopy.

Our results indicated that samples which were modified with hydroxyl scavengers corroded at a rate greater than or equal to that of unmodified BMI control samples. Optical and SEM microscopy of corroded samples revealed that the main mechanism of corrosion was stress corrosion cracking. Microcracks first initiated in the surface resin, then propagated along the fiber-matrix interface beneath the resin surface, resulting in the peeling and flaking of large fragments of uncorroded resin. In an effort to retard this mechanism, a sample containing epoxy-coated fibers was fabricated. It was postulated that the epoxy coating, which is resistant to galvanic corrosion, might prevent the microcracks from propagating along the fiber matrix interface, thus preventing flaking of the resin. While the preliminary effort using epoxy coatings did not succeed in reducing corrosion, other polymeric coatings may be helpful in attaining this objective and should be considered for this purpose.

# 2. INTRODUCTION

This report presents the results of the Phase I research undertaken by Foster-Miller, Inc. to demonstrate a novel approach to reducing galvanic corrosion in graphite/bismaleimide composites used in naval aircraft. In this section, background information is presented regarding galvanic-induced corrosion of imide-based polymers and how we approached a solution to this problem through the use of hydroxyl scavengers as modifiers for the imide resin. Following this introduction, Section 3 provides a full discussion of the experimental procedures, results, and conclusions obtained during the Phase I program. Section 4 presents a summary of the Phase I accomplishments and recommendations for future efforts.

## 2.1 The BMI Corrosion Problem

The degradation of imide polymers through hydrolysis by moisture or bases has been studied by a number of workers (3,4). Strong bases attack the imide group in the polymer structure and produce amic acid salts and amines.

In early 1990, at General Dynamics Fort Worth Division, it was discovered that imide-linked resins can degrade under certain laboratory conditions involving the galvanic process. The discovery was made while conducting solvent soak tests on composite materials (2). One of the solvents in the solvent-soak test matrix was aircraft sump water. This is a combination of 3 percent saltwater and jet reference fuel (5,6). Fluid containers used were one-gallon tin cans. Degradation in the form of resin loss resulting in loose fibers was observed after one day. The degradation initiated at composite edges and bare graphite fibers just above the saltwater interface.

The above laboratory experiment suggested that a galvanic process was occurring that produced hydroxyl groups. These hydroxyl groups subsequently attacked the imide linkage. Figure 1 illustrates the galvanic process that results in the base hydrolysis of the imide.

In Figure 1, metal ions go into solution sending electrons to the graphite cathode. This allows $OH^-$ ions to be generated at the graphite surfaces, in contact with the aqueous phase. The pH of the aqueous region above the interface is much higher than that of the bulk saltwater solution. This in effect served as a means of concentrating the hydroxyl ions in a confined area. This is a form of "crevice corrosion" (7). The pH in this area can be ~13, hence attack of the imide ring occurs resulting in the formation of an amide salt.

Based on the above understanding of the problem, the potential severity of galvanic induced degradation of imide based composites is greatest when the following conditions are met:

- Pooled or entrapped saltwater in contact with aluminum and graphite.
- Metal and graphite of composite in physical contact.
- Bare graphite of the composite at aqueous interface.

The imide based components currently in-service on naval aircraft where saltwater can potentially collect were shown in Table 1. In the future the degradation problem becomes more severe due to a projected increased use of imide based graphite composite structures.

At the Active Metal Anode:

$M \rightarrow M^{n+} + ne^-$

At the Graphite Cathode:

$O_2$ (dissolved) + $2H_2O$ + $2Na^+$ + $4e^- \rightarrow 4Na^+ + 4OH^-$

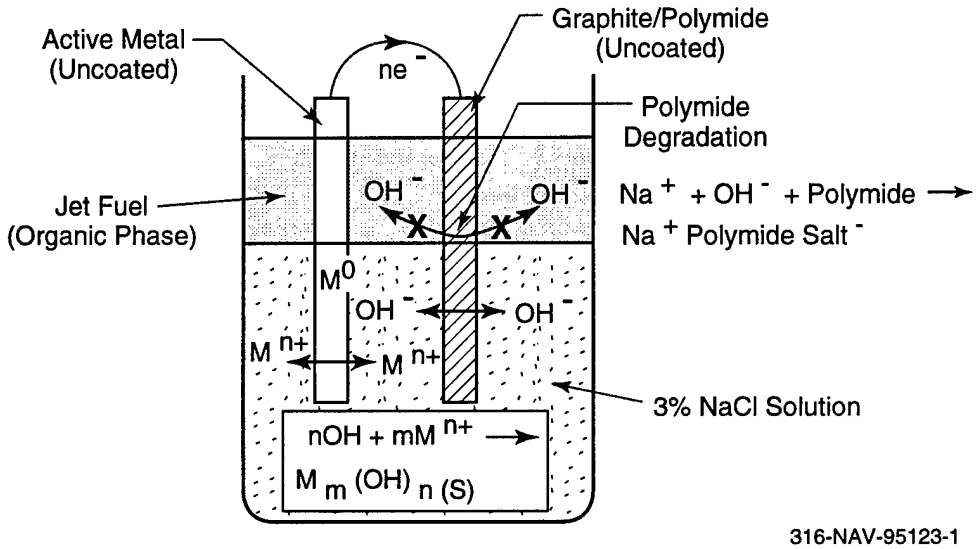


***Figure 1. Galvanic process that results in hydrolysis of an imide***

***Table 1. Locations for galvanic degradation of imide based composites***

| Aircraft | Potential Corrosion Location |
|---|---|
| F16XL | Wing skins |
| AV8B | Fuselage panels |
| A6/EA6 | Radomes |
| V22 | Engine fairings |

## 2.2 Foster-Miller's Approach to Preventing BMI Corrosion

The innovation pursued in this Phase I effort for the prevention of galvanic-induced degradation is based on using a hydroxyl group scavenger within the composite. This can be accomplished by 1) incorporating the hydroxyl scavenger into the backbone of the BMI resin or 2) use as an oligomer blended with pure BMI. Figure 2 illustrates this solution.

The selection of a hydroxyl scavenger was based on determination of the number of hydroxyl group equivalents produced during the galvanic corrosion process. We attempted to demonstrate the feasibility of the entire concept by fabricating test coupons, subjecting them to a laboratory galvanic process, and determining the bearing strength of the test coupons. The bearing strength is known to be sensitive to the degradation caused by galvanic corrosion (1). These test coupons were then compared to control test coupons to determine the extent of protection afforded by this approach.

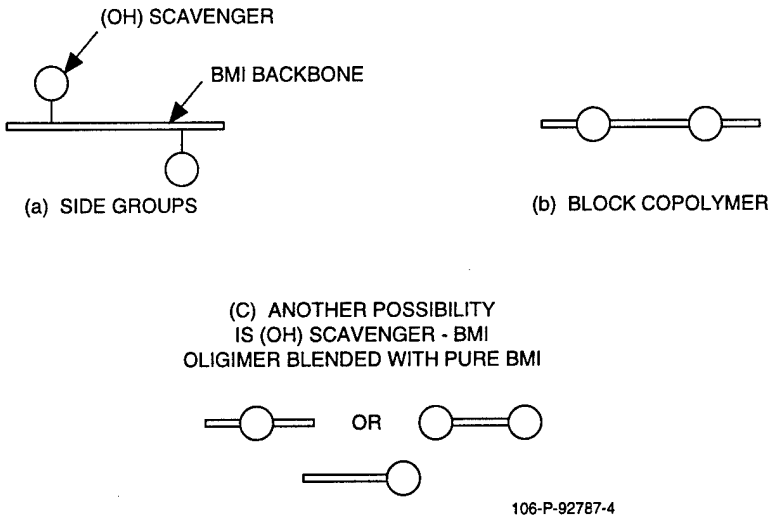


***Figure 2. Use of hydroxyl group scavengers to prevent corrosive attack from occurring***

# 3. EXPERIMENTAL PROCEDURES AND RESULTS

## 3.1 Research Objectives

The objective of this program was to establish the molecular mechanism of degradation of imide-based graphite composites when in contact with a corroding metal in an electrolytic saltwater solution. Once the mechanism was established, modifications to the BMI resin were investigated to evaluate a means to prevent the corrosive attack.

Specific goals of the Phase I program were to:

- Establish mechanism of hydroxyl attack of BMI.
- Evaluate means to prevent corrosive attack.
- Select modifications for imide based resins.
- Fabricate modified graphite fiber reinforced BMI test coupons.
- Test bearing strength of modified test coupons before and after exposure, with and without modified resin.

## 3.2 Procedures and Results

In this section, the results obtained for each of the tasks performed are presented along with the descriptions of experimental procedures and apparatus. There are five experimental subsections, as described below:

- 3.2.1 Determination of the upper and lower bounds of the rate of corrosion.
- 3.2.2 Selection of hydroxyl scavengers for modification of the BMI resin.
- 3.2.3 Fabrication of composite test coupons.
- 3.2.4 Corrosion of test coupons in a jet fuel - 3 percent saltwater mixture while attached to an aluminum post.
- 3.2.5 Characterization of corrosion in test coupons via DRIFT infrared spectroscopy, optical microscopy, and SEM microscopy.
- 3.2.6 Measurement of the bearing strength of corroded test coupons.

### 3.2.1 Determination of the Rate of Corrosion

#### 3.2.1.1 Corrosion Rate Experiment

Control test specimens were fabricated using Narmco 5250-4 Bismaleimide (BMI) resin with 24 plies of AS-4 graphite fiber fabric in a 0 deg/90 deg orientation. Fiber volume fraction was

near 60 percent. To determine the upper limit of the corrosion, one specimen was corroded in pH 14 NaOH solution for 28 hr and was weighed before and after corrosion. The purpose of this was to raise the overall concentration of hydroxyl groups to as high a value as possible to enhance corrosion rate. Table 2 shows the weight before and after corrosion for two test specimens.

***Table 2. Upper limit corrosion in pH 14 NaOH solution***

| | Weight Before (g) | Weight After (g) | Rate of Corrosion (mm/year) |
|---|---|---|---|
| Specimen 1 | 12.83 | 12.82 | 0.58 |
| Specimen 2 | 12.74 | 12.73 | 0.63 |

To determine the lower limit, another specimen was corroded galvanically. This specimen was connected to an aluminum anode and corroded in a 3.5 percent NaCl solution for 24 hr. The average current was measured by setting up a galvanic couple between an aluminum electrode and the control composite sample. A zero-resistance ammeter was connected between the two samples using a titanium bolt to provide electrical contact to the graphite composite. The experimental setup is shown in Figure 3. The current was monitored every 5 min for a period of 1 hr at both the beginning of the corrosion and at 19 hr (Figure 4). The current indicated in Figure 4 was an average of these measurements. Table 3 shows the weight loss and the average current (with standard deviation) measured.

These tests provided apparently anomalous results. In particular, the rate of corrosion for the samples in pH 14 NaOH solution (which should have provided an upper limit on corrosion rate) was determined to be an average of approximately 0.603 mm/year, whereas it was calculated to be approximately 1.42 mm/year for the sample in the lower limit 3 percent saltwater solution. One problem is that the accuracy of these measurements is limited by

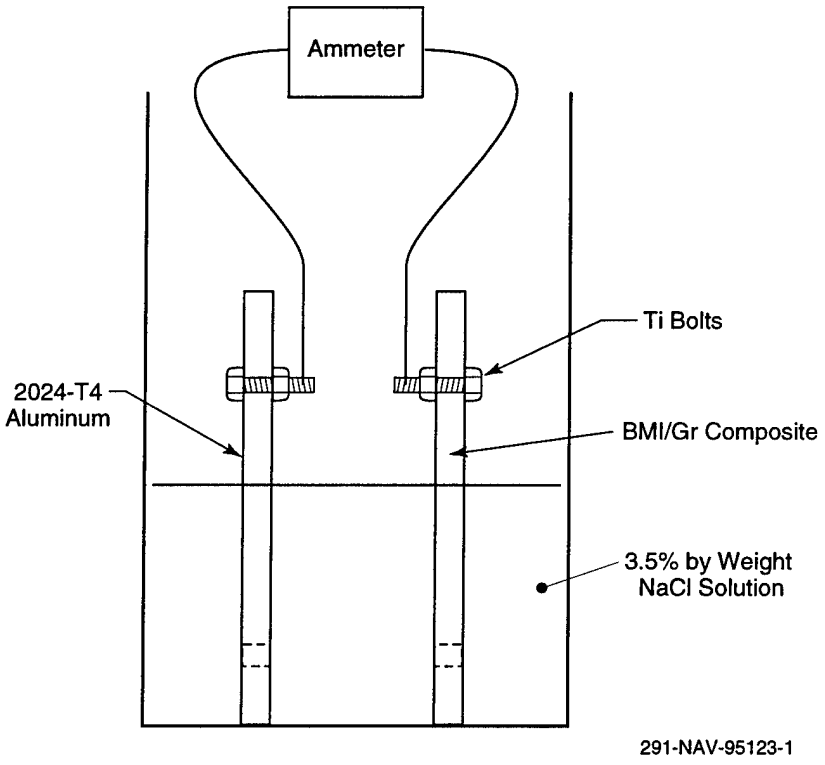


***Figure 3. Experimental galvanic cell setup for monitoring corrosion rate***

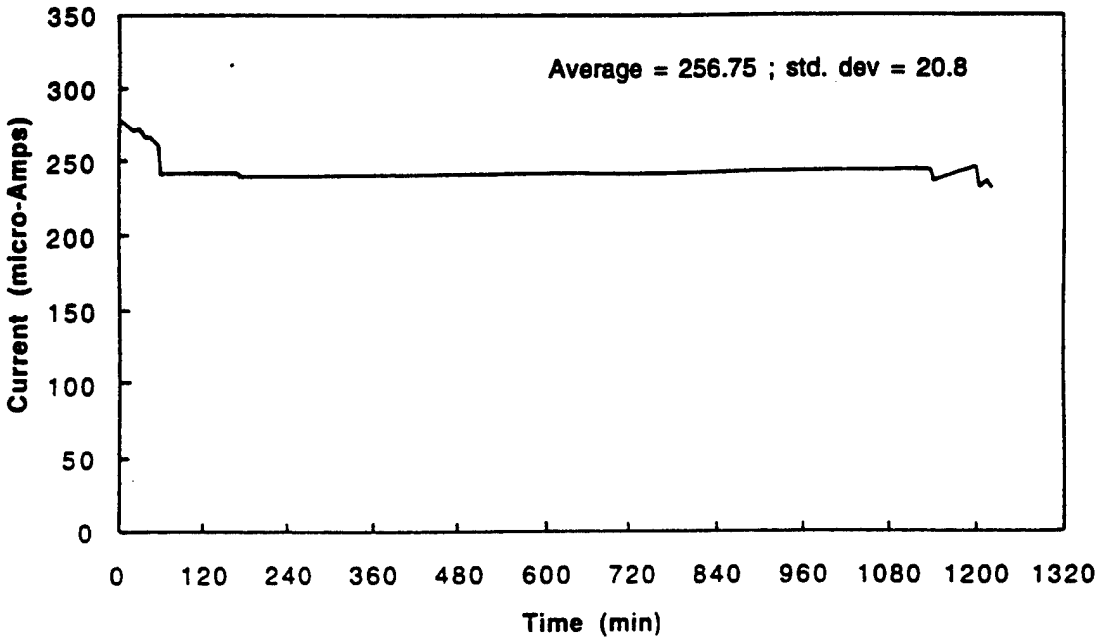


***Figure 4. Galvanic current as function of time***

measurement error resulting from moisture uptake into the composite. Although efforts were made to dry the samples thoroughly before and after each experiment, the amount of moisture retained by the composite was difficult to control. The specimens were even staged in an oven for 24 hr at 150°C after experimentation to eliminate moisture and reach an equilibrium value. Nevertheless, despite the fact that these precautions were taken and the measurements represent the highest level of accuracy possible under the circumstances, their error is still inherently high. This would explain in part why the lower corrosion limit actually exceeds the upper corrosion limit.

***Table 3. Lower limit corrosion in 3.5 percent NaCl solution***

| | |
|---|---|
| Weight before (g) | 12.394 |
| Weight after (g) | 12.380 |
| Average current (μA) | 256 ± 21 |
| Rate of corrosion (mm/year) | 1.42 |

Another factor that may be important relates to the effective concentration and distribution of hydroxyl ions in the solution. The average current measured from the galvanic couple predicts an average surface concentration of hydroxyl groups to be nearly equal to that of the pH 14 NaOH solution. This may explain the small weight loss difference between the two corrosion experiments. The lower rate of corrosion in the pH 14 NaOH solution may be due to localized depletion of hydroxyl groups in the composite surface region, whereas in the galvanic couple a constant supply of hydroxyl groups are produced at the surface.

In both experiments, weight loss measurements indicated that two-thirds of the hydroxyl groups produced by the galvanic process (or available in solution) attacked the bismaleimide.

These data were subsequently used to predict the weight percent of hydroxyl scavenger additives needed to prevent corrosion for a specified period of time. This effort, and the scavengers that were selected, are described later in this report.

### 3.2.2 Selection of Hydroxyl Scavengers

The control BMI resin chosen for this study was Narmco 5250-4 which is available from Cytec Engineered Materials. Several additional resins were identified as possible hydroxyl scavengers for use in modifying the control BMI resin. The parameters used to select these scavengers were:

- Presence of acidic phenolic hydroxyl (OH) groups which could scavenge.
- Expected solubility in BMI.
- Ability to cure to a thermally stable resin with good mechanical properties at a similar cure temperature to the BMI.
- Availability as a low cost powder.

The candidate scavengers chosen for this study are summarized in Table 4. The first hydroxyl scavenger chosen was Diallyl Bisphenol A (DABPA), which has two scavenger sites per molecule. Matrimid® 5292 is a commercially available two-part resin system made up of 4,4'-Bismaleimidodiphenylmethane and o,o'-Diallyl Bisphenol A. The maximum mechanical properties can be obtained by mixing these two components in a 1.31 to 1 parts by weight ratio of the bismaleimide to the Diallyl Bisphenol A. This results in a scavenger to susceptible imide linkage ratio of 1/20. The Diallyl Bisphenol A component of Matrimid 5292 was also used to modify the control BMI resin, although this blend was not used for composite studies. In the table, "hexa" refers to hexamethylenetetramine catalyst.

A resole resin, two novolac resins, and two resorcinol/formaldehyde resins were also identified. The resole resin has one scavenger site per monomer molecule, whereas the resorcinol/formaldehyde has two. Figure 5 shows the molecular structure of the three scavengers chosen as initial modifiers.

***Table 4. Candidate hydroxyl scavengers and their solubility in Narmco 5250-4 BMI***

| Scavenger | Scavenger Type | Weight % Scavenger | Solubility |
|---|---|---|---|
| Plenco 12505 | Novolac (no hexa) | 5% to 20% | Blended readily at 140°C |
| Plenco 12477 | Novolac (w/hexa) | 5% to 20% | Hexa not soluble |
| Plenco 11885 | Resole (1 stage) | 5% to 20% | Gelled rapidly - insoluble |
| Matrimid 5292 Part "B"* | Diallyl Bisphenol A | 20% to 46% | Blended readily at 130°C |
| Penacolite B-1A | Resorcinol-Formaldehyde | 5% to 20% | Blended readily at 140°C |
| Penacolite B-20-S | Resorcinol-Formaldehyde | 5% to 20% | Blended readily at 140°C |

* In the remainder of this report, "Matrimid" shall refer to Matrimid 5292, and not to the control BMI/Matrimid Part B blend, unless otherwise noted.

To evaluate these scavengers, several tests were conducted. Solubility studies were conducted to determine the compatibility of these systems with the control BMI resin, DSC studies were used to evaluate the Tg of cured samples, and flexural studies on clear castings provided mechanical properties of the cured blends.

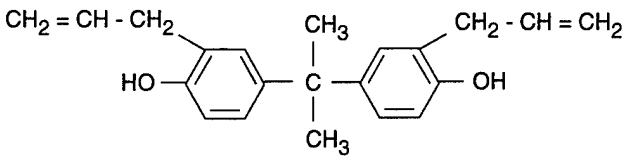


Diallyl Bisphenol A

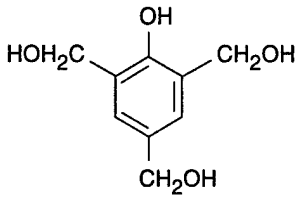


Resole Resin

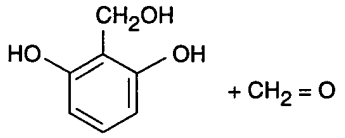


Resorcinal/Formaldehyde Resin

291-NAV-95123-3

***Figure 5. Identified hydroxyl group scavengers***

### 3.2.2.1 Solubility Studies

Solubility studies were performed by blending the scavengers into the Narmco 5250-4 BMI at loadings ranging from 5 to 20 percent by weight. For the Diallyl Bisphenol A samples, loadings between 20 percent and 46 percent were investigated, using recommendations from the manufacturer's literature (again, in the remainder of this report, "Matrimid" refers to Matrimid 5292 and not to the control BMI/Matrimid Part B blend, unless otherwise noted). Blending was done manually in test tubes in the range 130° to 140°C. Results of the blending study are summarized in Table 4. All systems blended easily into the BMI system under these conditions, with the exception of the resole resin and the novolac system containing a hexa-methylenetetramine (hexa) catalyst. The resole resin was found to gel rapidly in the BMI, even at temperatures as low as 80°C, which is the minimum temperature at which powders can be blended into BMI. In the novolac/hexa system, the novolac dissolved easily into the BMI, while the hexa catalyst remained as a precipitate.

### 3.2.2.2 Fabrication of Clear Castings

Clear castings of the blended resins were cured for use in the flexural and DSC studies. For all systems except the BMI/resole blend, samples were cast into 2 in. diameter discs approximately 0.05 in. to 0.08 in. thick. Samples were degassed under vacuum for 15 min at 135°C, then cured at 175°C for 6 hr, followed by a post-cure at 225°C overnight. These were sanded smooth, then cut into samples 0.4 in. wide for flexural testing. Additional sample material, broken from the edges of the discs, were prepared for DSC testing.

### 3.2.2.3 DSC Testing of Clear Castings

DSC testing was performed to evaluate the effect of the scavengers on the Tg of the cured resins and to identify any phase separation that might have occurred. Two scans were run, with Tg being taken from the second scan. DSC scans were run to 320°C at 50°C/min to accentuate the glass transition signal. Results are summarized in Table 5. As can be seen, the Tg of all the modified systems (with the exception of the BMI/resole blend) was lower than that of the unmodified BMI. It is important to note that Tg measured via this technique was not

*Table 5. Glass transition temperatures for modified BMI systems from DSC studies*

| Resin Formulation | Scavenger Type | Tg (°C) |
|---|---|---|
| Narmco 5250-4 (BMI Control) | None | 302 |
| Matrimid 5292 (46% Part "B") | Diallyl Bisphenol A | 231 |
| BMI & 46% Matrimid Part "B" | Diallyl Bisphenol A | 207 |
| BMI & 20% Plenco 12505 | Novolac (w/hexa) | 274 |
| BMI & 20% Plenco 11885 | Resole (1 Stage) | 305 |
| BMI & 20% Penacolite B-20-S | Phenol-Formaldehyde | 269 |
| BMI & 20% Penacolite B1A | Phenol-Formaldehyde | 292 |

necessarily the Tg of the cured resins, since postcuring of the resins occurred during the first heatup. However, since all samples were heated in a similar fashion, these Tg values should provide relative data for comparison purposes. None of the systems showed any signs of phase separation.

#### 3.2.2.4 Flexural Testing of Clear Castings

Flexural testing was performed on a Universal testing machine using a three point flexural testing fixture. A 1 in. span was used for all tests, with a crosshead speed of 0.05 in./min. Due to a limited sample size, only one to two samples were available for each test group. Results of the flexural testing are summarized in Table 6. All modified samples exhibited lower strengths and failure strains than the unmodified BMI samples. The BMI/20 percent Plenco 12477 (novolac with hexa catalyst) sample exhibited extremely poor strength due to the undissolved hexa inclusions in the resin. Within experimental error, all other modified samples exhibited similar strength and strain to failure.

### 3.2.3 Fabrication of Composite Test Coupons

Based on the combined results of the solubility, DSC, and flexural studies, three of the scavengers were chosen for composite corrosion studies. These included the Matrimid 5292 (BMI/Diallyl Bisphenol A), Narmco 5250-4/20 percent Plenco 12477 (BMI/novolac, but without hexa catalyst), and Narmco 5250-4/20 percent Penacolite B-1A (BMI/resorcinol-formaldehyde) blends. For the final modified system, the Narmco 5250-4 resin was used in conjunction with epoxy coated carbon fiber fabric (as will be discussed later). The systems chosen for composite fabrication are summarized in Table 7.

Composite panels were fabricated using a six ply $[90]_{3S}$ layup of 375 g/m$^2$ 8HS woven carbon fiber fabric. Each ply of this fabric is essentially equivalent to a [90/0] prepreg layup, providing a layup similar to $[90/0]_{3S}$. The panel size was 12 in. x 12 in. During fabrication, an excess of resin was placed in thin sheets between alternating plies of the fabric. Following vacuum bagging, the resin was infused into the fabric under vacuum during the heating stage of the cure cycle. Excess resin was then squeezed into a bleeder ply under 140 psi pressure. The panels were cured according to the manufacturer's recommended cure schedule of 175°C for at least 6 hr, followed by a free-standing postcure at 225°C for 6 hr. A target fiber volume

*Table 6. Results of three-point bend flexural testing on resin clear castings*

| Resin Type | Maximum Stress (ksi) | Maximum Strain | Observations |
|---|---|---|---|
| Narmco 5250-4 (BMI control) | 25.3 | 5% | |
| BMI & 20% Plenco 12505 | 19.4 | 4% | |
| BMI & 20% Plenco 12477 | 5.8 | -- | Contained Hexa Inclusions |
| BMI & 46% Matrimid B | 23.8 | 4% | |
| BMI & 20% Penacolite B-1A | 14.1 | 4% | Slightly Damaged Samples |
| BMI & 10% Penacolite B-20-S | 23.2 | 4% | |
| BMI & 20% Penacolite B-20-S | 19.8 | 3-4% | |
| Matrimid 5292 (46% B) | 19.8 | 4-7% | |

*Table 7. Resin formulations chosen for composite corrosion studies and the weight change noted after 96 hr of corrosion*

| Resin Formulation | Experimental Condition | Average Weight Change | Standard Deviation |
|---|---|---|---|
| Narmco 5250-4 (BMI) | Control | +0.52% | 0.11% |
| Matrimid 5292 (46% Part "B") | Diallyl Bisphenol A | +0.99% | 0.24% |
| BMI/20% Plenco 12505 | Novolac (no hexa) | +1.31% | 0.27% |
| BMI/20% Penacolite B-1A | Resorcinol-Formaldehyde | -0.12% | 0.15% |
| Narmco 5250-4 (BMI) | Epoxy coated fibers | +0.29% | 0.13% |

fraction of 60 percent was chosen. For all but the epoxy coated fiber panel, fiber volume fraction ranged between 62 percent and 68 percent; for the epoxy coated fiber panel, fiber volume fraction was approximately 50 percent due to difficulties compacting the epoxy coated fabric.

For the epoxy coated fiber panel, a thin coating of Araldite MY720 (TGDDM epoxy)/DDS was first applied to the fiber surface via a solution coating method and cured. During solution coating, a solution of acetone and MY720/DDS epoxy was applied to the carbon fiber fabric and the acetone was allowed to evaporate, leaving a thin coating of epoxy resin on each fiber. Next, the epoxy was cured for 3 hr at 175°C. Curing was conducted under vacuum to avoid oxidation of the thin epoxy coating. To determine the appropriate concentration of epoxy in the coating solution, trials were conducted using 0.5 to 4 percent epoxy by weight. Samples coated using a solution of 1 percent epoxy by weight were found to provide an adequate coating without causing excessive agglomeration of the fiber tows. For the composite panel, six plies of fabric were coated using a 1 percent solution and cured. The composite was fabricated as

noted above, except that an overnight postcure temperature of 200°C, instead of the normal 225°C, was used to prevent thermal degradation of the epoxy.

Composite panels were cut into test coupons using a diamond tipped saw. The test coupon geometry was modified from that described in the proposal in order to position the corrosion line at the bolt hole (for bearing strength testing) and to remove excess material from the sample. The new sample geometry, 1 in. x 3 in., is shown in Figure 6a. Two holes were drilled using a 3/16 in. carbide spade bit.

### 3.2.4 Corrosion of Test Coupons

Six cut and drilled composite samples were fastened to aluminum strips (1/8 in. thick x 1 in. wide x 3 in. long) using titanium bolts and nuts as shown in Figure 6b. Corrosion of these samples was conducted in a closed vessel, as shown in Figure 7. A 50/50 mixture of 3 percent saltwater and Jet A jet fuel was prepared such that the water-fuel interface was positioned at the center of the upper bolt hole. This caused corrosion in the immediate vicinity of the hole where bearing strength was to be tested, as shown in Figure 6c. The corrosion temperature was controlled by immersing the corrosion chamber in a constant temperature bath.

In preliminary studies, a BMI composite control sample was corroded for 24 hr at room temperature. This resulted in no noticeable corrosion. Following literature reports (1-3), we changed the test temperature to 80°C. Control and Matrimid samples, corroded at 48 hr, showed significant corrosion but a small reduction in bolt bearing strength. Control samples, corroded at 80°C for 96 hr, showed both substantial corrosion and reduction in bearing strength. Thus, for all remaining samples, corrosion was conducted at 80°C for 96 hr.

Before corrosion, samples were dried under vacuum at 100°C for 5 hr and weighed. After corrosion, samples were rinsed with water and dried according to the same schedule. Weight change results are summarized in Table 7. All except the BMI/Phenol-Resorcinol-Formaldehyde samples, where corrosion was particularly severe, showed a slight weight gain, despite the apparent removal of resin from the corrosion region. This weight gain is probably due to irreversible moisture absorption by the resin during corrosion. Moisture uptake by the BMI is not unexpected, as manufacturer's literature for the Narmco 5250-4 system reports 4.2 percent weight gain in the neat resin after 1000 hr of exposure at 71°C.

Visual observation of all corroded samples indicated that all modified systems corroded at a rate equal to or greater than that of the BMI control system. Five corroded samples from each experimental condition were retained for bolt bearing strength testing, while one sample was saved for optical microscopy and DRIFT infrared spectroscopy.

### 3.2.5 Characterization of Corrosion in Test Coupons

Three techniques were used to characterize the corrosion of the test coupons. DRIFT infrared spectroscopy was used to identify the chemical reactions occurring in the corrosion regions of the samples. Optical microscopy was used to examine the extent of degradation and to determine mechanisms of corrosion. SEM microscopy was used to confirm some of the preliminary findings from the optical microscopy study.

#### 3.2.5.1 DRIFT Infrared Spectroscopy

One sample from each experimental condition was spectroscopically characterized by DRIFT. Spectral data was taken at one point on each sample. For the corroded samples, spectra were taken from within the corroded region. Spectra from each of the sample types are shown in Figures 8a to 8e.

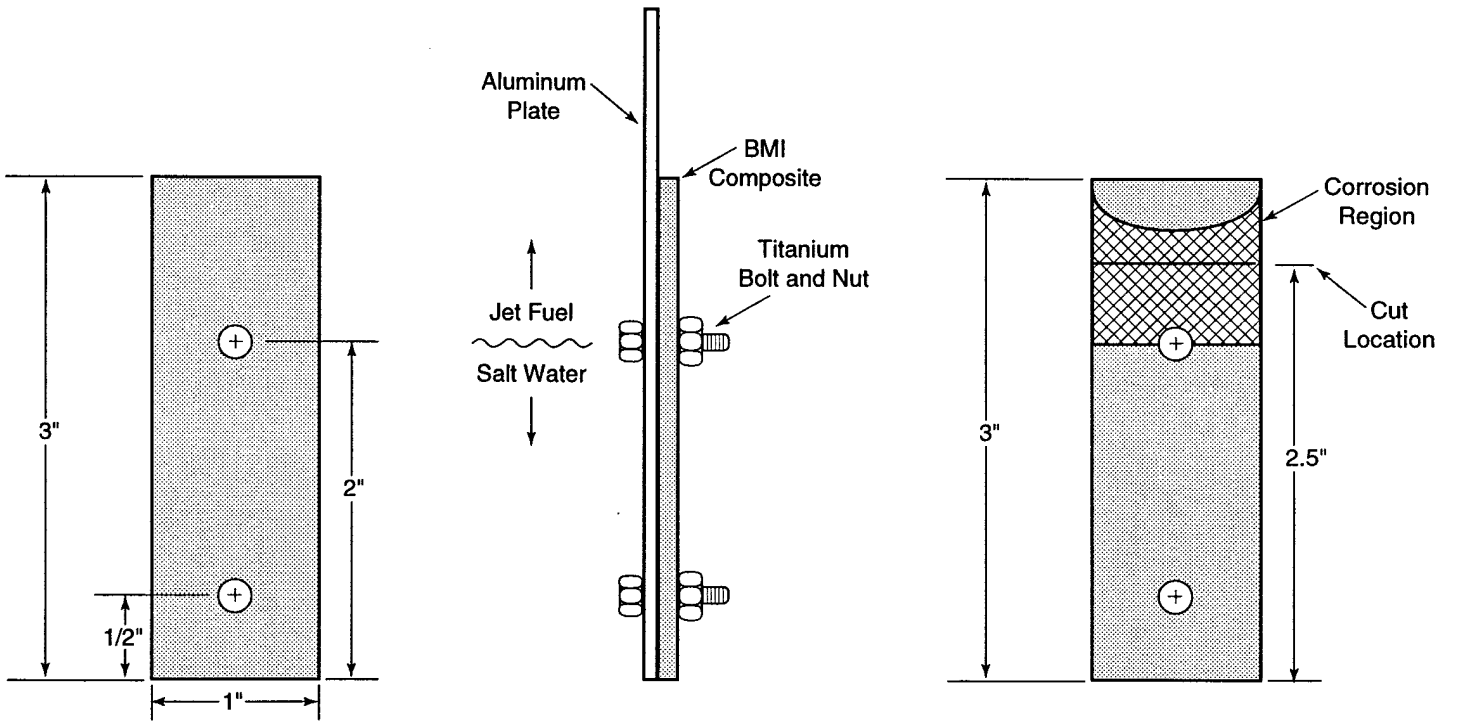


***Figure 6. Composite sample for corrosion experiment***

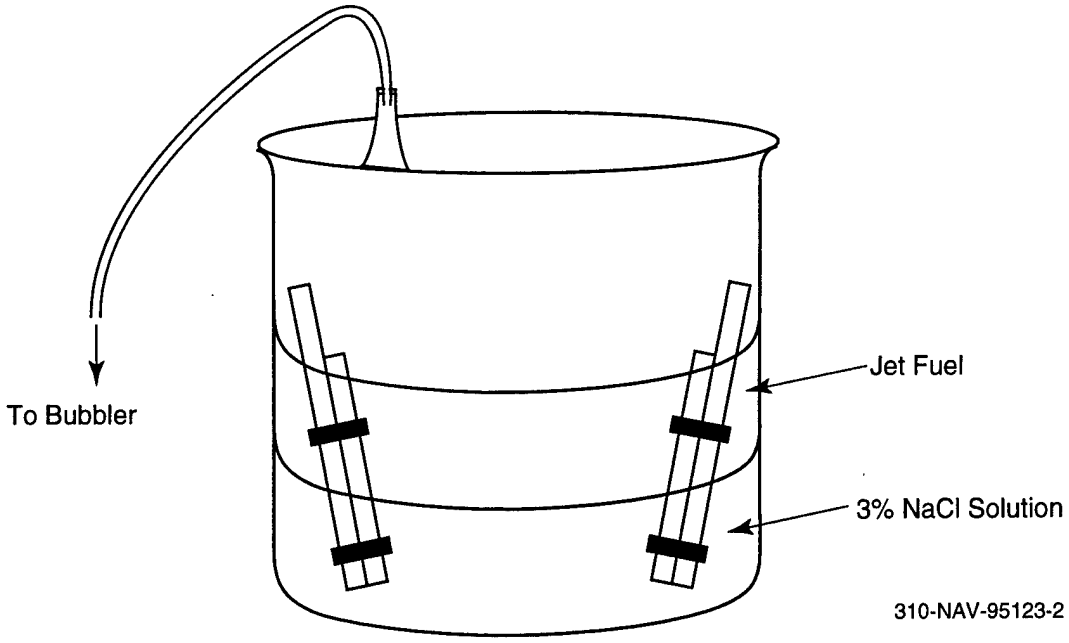


***Figure 7. Corrosion bath setup***

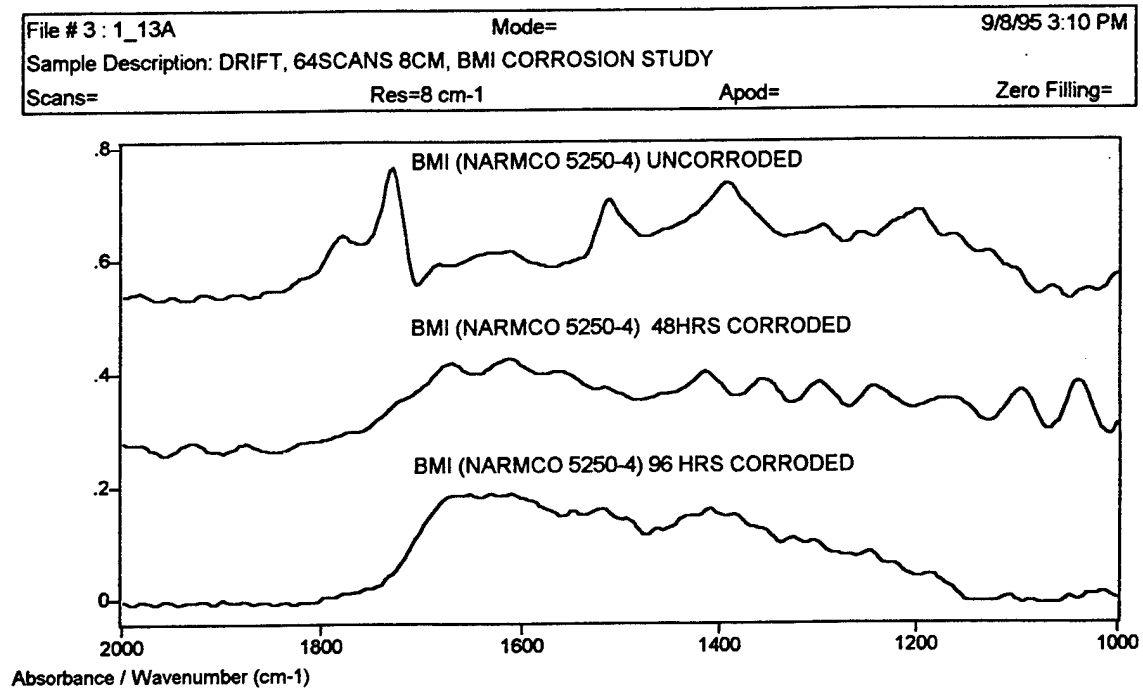


***Figure 8a. Stacked spectral plots of BMI control samples in uncorroded, 48 hr corroded, and 96 hr corroded conditions***

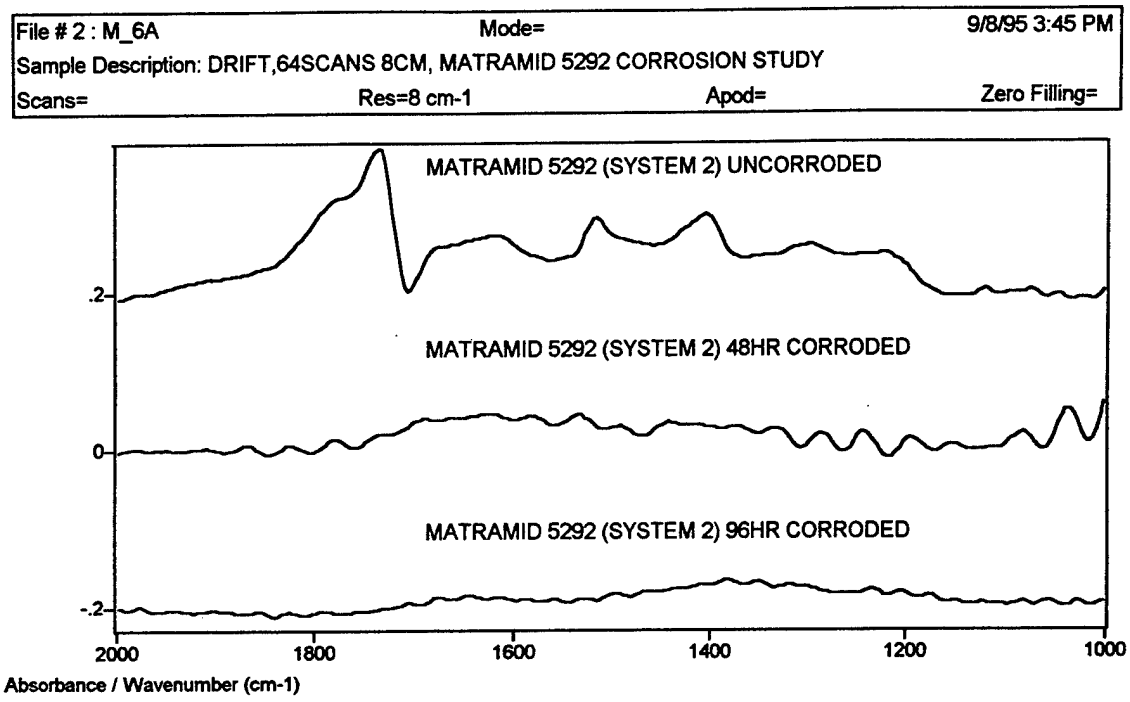


***Figure 8b. Stacked spectral plots of Matrimid samples in uncorroded, 48 hr corroded, and 96 hr corroded conditions***

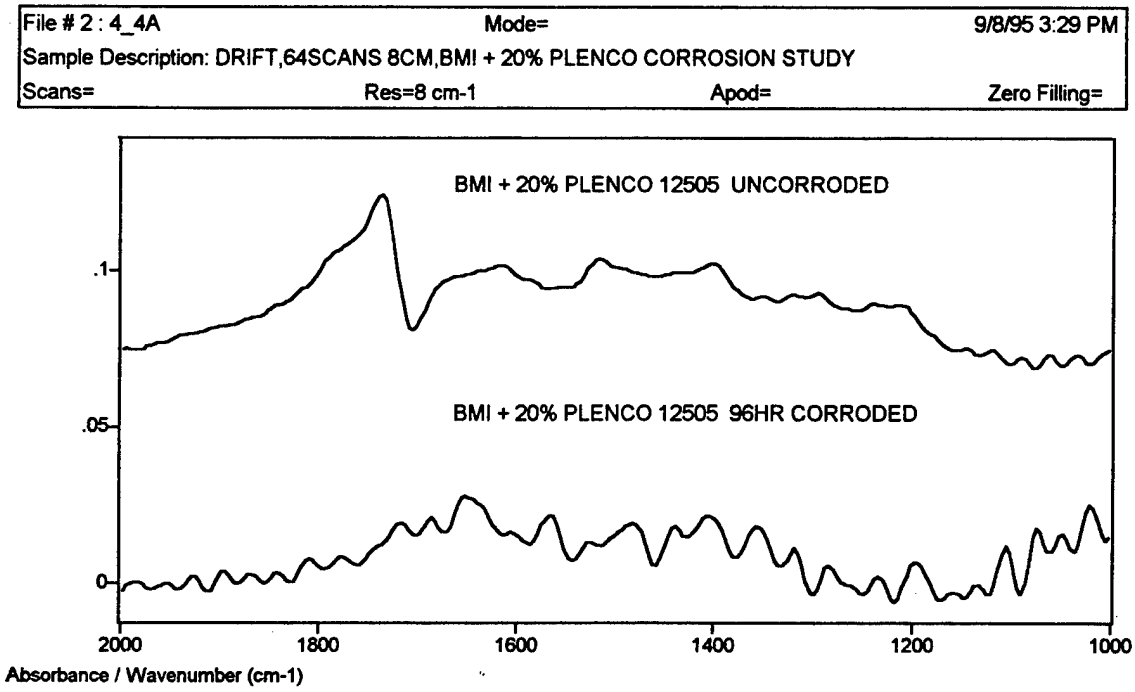


***Figure 8c. Stacked spectral plots of Plenco 12505 modified samples in uncorroded and 96 hr corroded conditions***

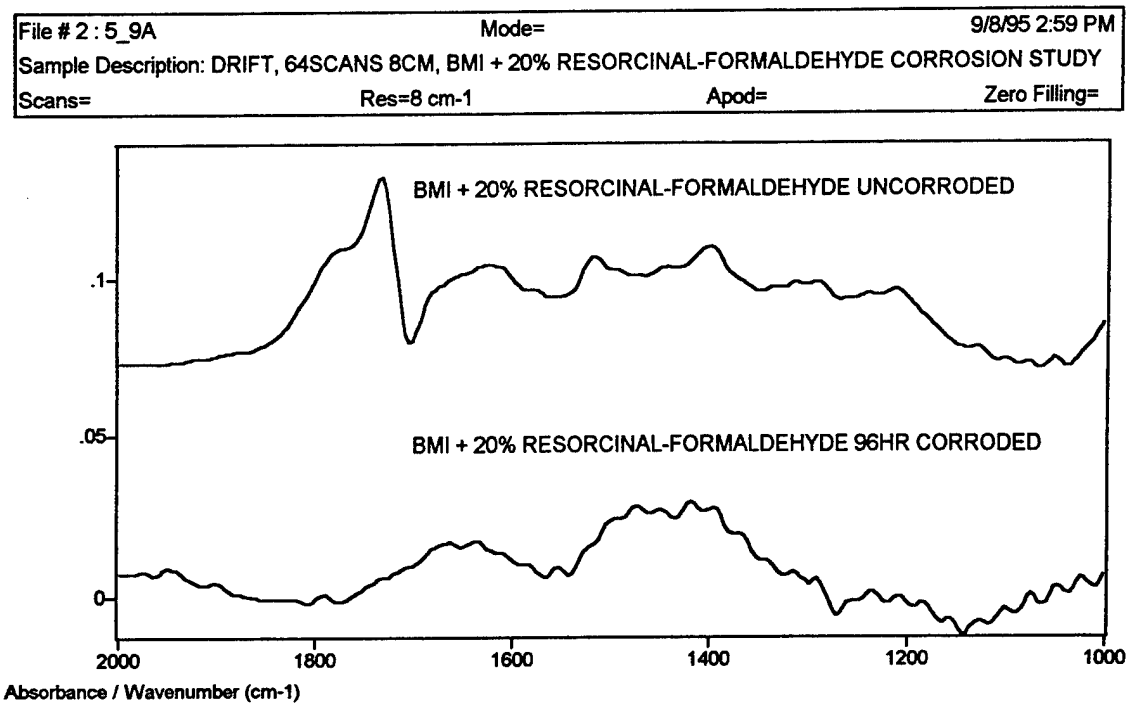


***Figure 8d. Stacked spectral plots of Penacolite B-1A modified samples in uncorroded and 96 hr corroded conditions***

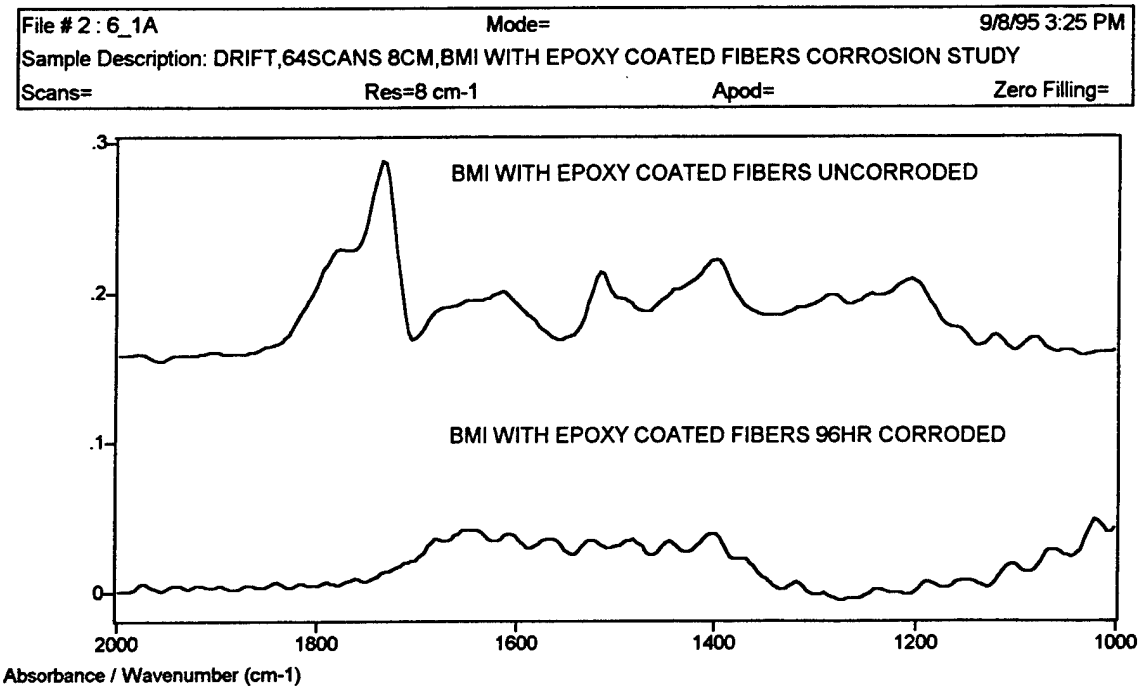


***Figure 8e. Stacked spectral plots of epoxy coated fiber samples in uncorroded and 96 hr corroded conditions***

The spectra from all samples are very similar. All exhibit decay of the imide ring, which absorbs at 1733 $cm^{-1}$, and formation of the carboxylic acid moiety at 1650 $cm^{-1}$. These features indicate similar degradation mechanisms in all samples. From these results, it does not appear that the scavengers had any effect on the degradation mechanism.

#### 3.2.5.2 Optical Microscopy

Photographs of samples which were corroded 96 hr at 80°C are shown in Figure 9a. The size and shape of the corroded regions for each sample are illustrated in Figure 9b. An uncorroded BMI sample is shown for comparison. Higher magnification views of each sample are shown in Figures 10a to 10e. The BMI control, Matrimid and epoxy coated fiber samples showed the lowest levels of visible corrosion, while the samples modified with Plenco 12505 and Penacolite B-1A showed slightly higher levels of visible corrosion.

Photographs of BMI control and Matrimid samples which were uncorroded, corroded for 48 hr, and corroded for 96 hr are shown in Figure 11a. The size and shape of the corroded regions for each sample are illustrated in Figure 11b. The "U" shaped corrosion front on the 48 hr corrosion samples indicates that corrosion progressed quicker up the edges of the sample than in the center. Since the fibers in the outermost plies of the fabric were oriented horizontally, it is likely that corrosion propagated from the edges of the sample inward along the fiber direction.

Optical microscopy was performed on BMI control and Matrimid samples which had been corroded for 48 hr. The areas of these samples which were examined, shown in Figure 12, were primarily near the corrosion front above the saltwater-jet fuel interface.

Under optical microscopy, all samples showed similar mechanisms of corrosion. In general, corrosion was observed to initiate from exposed fibers at the drilled hole and at the edge of the sample. In the center of the corroded region, the fibers were almost completely bare (Figure 13). At the corrosion front, significant matrix cracking was noted, mostly in the direction of fiber orientation. This is seen in Figure 14a, in a region of a control BMI sample corroded for 48 hr. Here, in the locally thick resin region where the fiber tow dives into the weave structure, microcracking is very visible. When compared to the uncorroded control sample in Figure 14b, it is apparent that this microcracking is due to the corrosion process, as it is not visible in the control. This microcracking, combined with the absence of pitting on the resin surface, suggests that the mechanism by which corrosion advances is stress corrosion cracking. Here, the residual tensile stresses in the matrix, due to CTE mismatch between the resin and fiber, drive the crack propagation. Most corrosion occurs locally at the crack tip due to chemo-mechanical mechanisms.

Following microcracking, the resin appears to flake off of the composite surface, rather than etching away. This is seen in Figure 15, where strips of resin are seen peeling away from the surface. This implies that after initiating microcracks, corrosion progresses locally along the fiber-matrix interface. By this mechanism, the crack tunnels beneath the resin surface, causing relatively large fragments of uncorroded resin to be removed from the surface of the composite.

A view of the edge of the control sample corroded for 48 hr is shown in Figure 16. On the outermost ply (in the surface corrosion region), loose fibers are seen. Deeper into the sample, few loose fibers are visible. Instead, delamination occurs across the thickness of the exposed edge, although it is difficult to determine the depth to which these delaminations propagate. The mechanism of delamination is not as clear as the mechanism of resin removal on the corroding surface, although it is likely that stress corrosion cracking is involved.

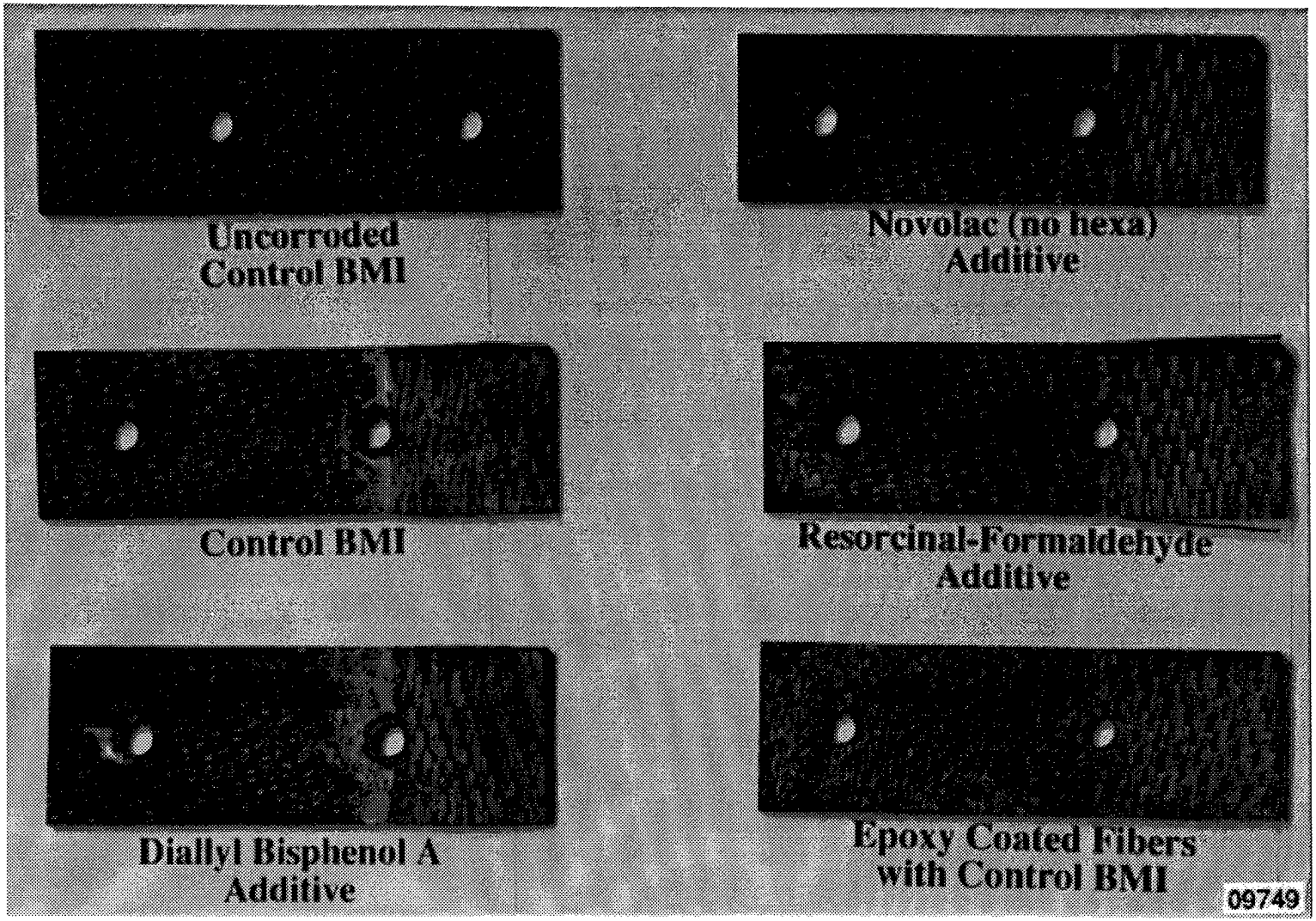


*Figure 9a. Photos of uncorroded control sample and all sample types corroded for 96 hr at 80°C*

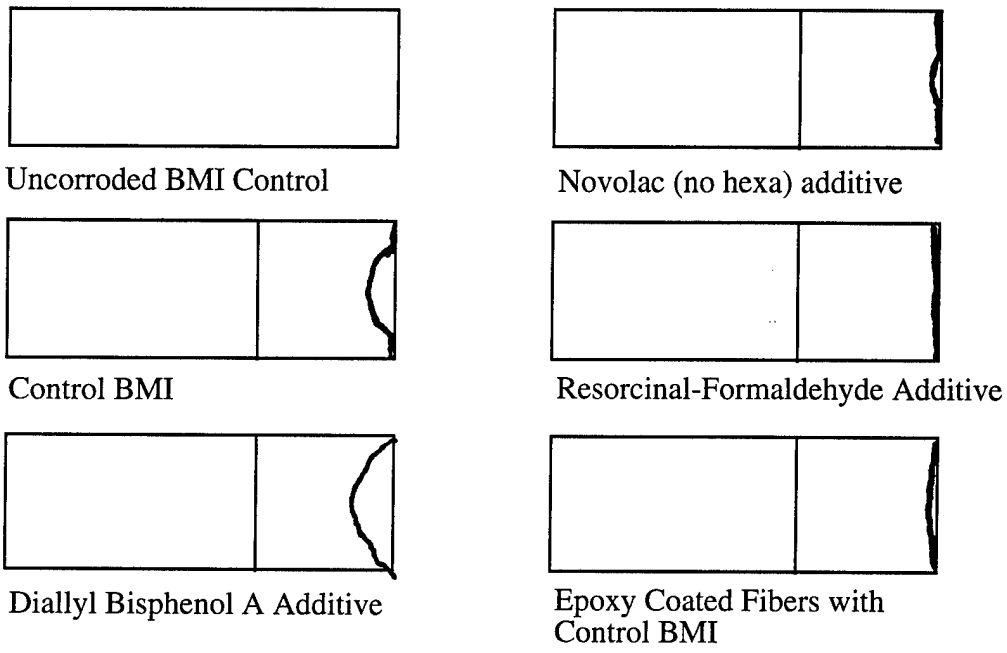


***Figure 9b. Illustration of the size of the corroded region for the samples in Figure 9a***

### 3.2.5.3 SEM Microscopy

SEM microscopy was conducted to verify optical microscopy observations. Since optical microscopy had indicated that all samples showed similar mechanisms of corrosion, only two experimental groups, the control and the Matrimid samples, were investigated. Uncorroded samples, as well as samples corroded for 48 and 96 hr, were examined. While most of the optical micrographs were taken in the highly corroded region above the saltwater-jet fuel interface, SEM examination indicated that similar features were present both at the corrosion front (above the saltwater-jet fuel interface) and below the interface, where the composite was exposed to the saltwater solution. Since the features below the interface were more pronounced, SEM microscopy was focused there instead of at the corrosion front. A legend showing SEM micrograph locations is shown in Figure 17.

Figure 18 shows uncorroded control, 48 hr corroded control, and 48 hr corroded Matrimid samples at 130x. Figures 18b and 18c are taken well below the saltwater-jet fuel interface. Microcracking along the fiber direction is evident in both of the corroded samples. Similar regions from these samples, taken at 360x, are shown in Figure 19. A 1600x view of a region where microcracks are initiating in the 48 hr corroded sample is shown in Figure 20. The surface texture present here appears to be deposits of salts and corrosion by-product, and not pitting, since it is absent in other corroded areas. The small cracks appear to be propagating slowly until they reach a critical size. Unlike the microcracks in Figure 18, the edges are rough, as if caused by chemical degradation. The straight, smooth cracks in Figure 18 are more indicative of rapid, unstable crack growth, which probably occurred when initiating microcracks reached a critical size.

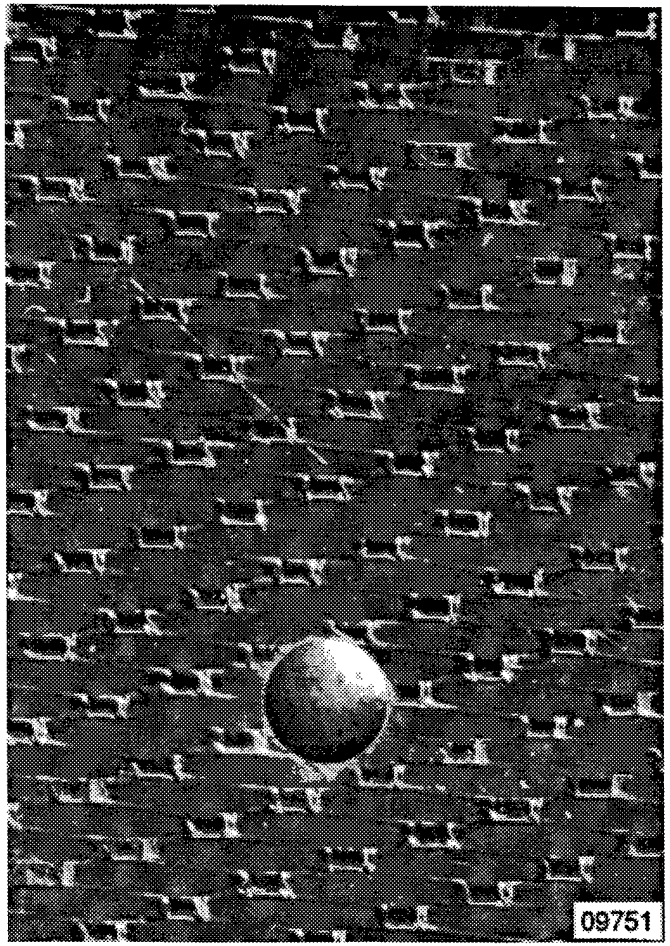


*Figure 10a. Close-up view of an uncorroded BMI control sample*

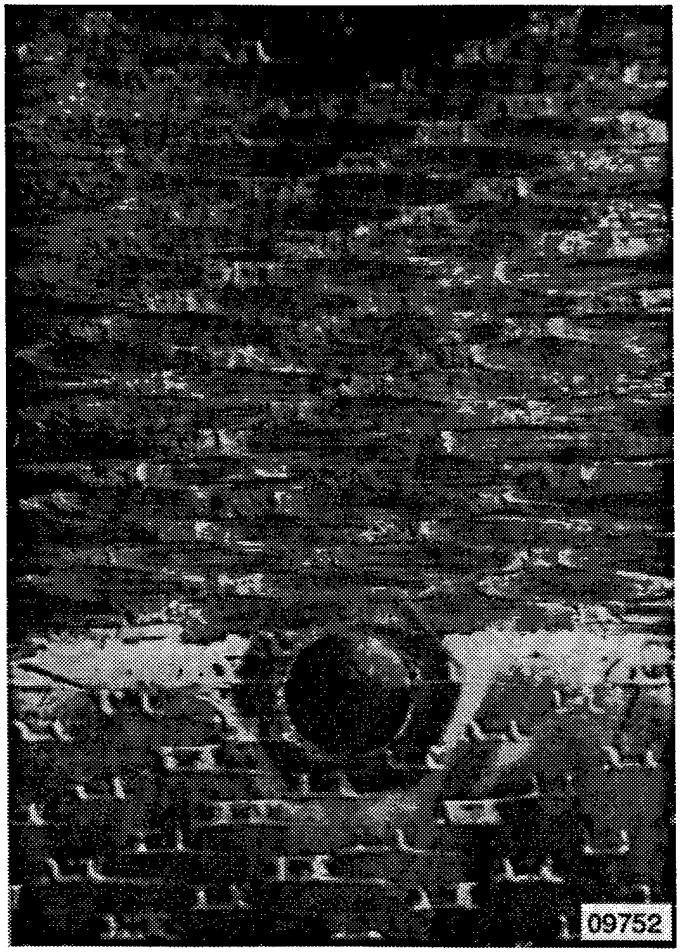


*Figure 10b. Close-up view of a BMI control sample corroded 96 hr at 80°C*

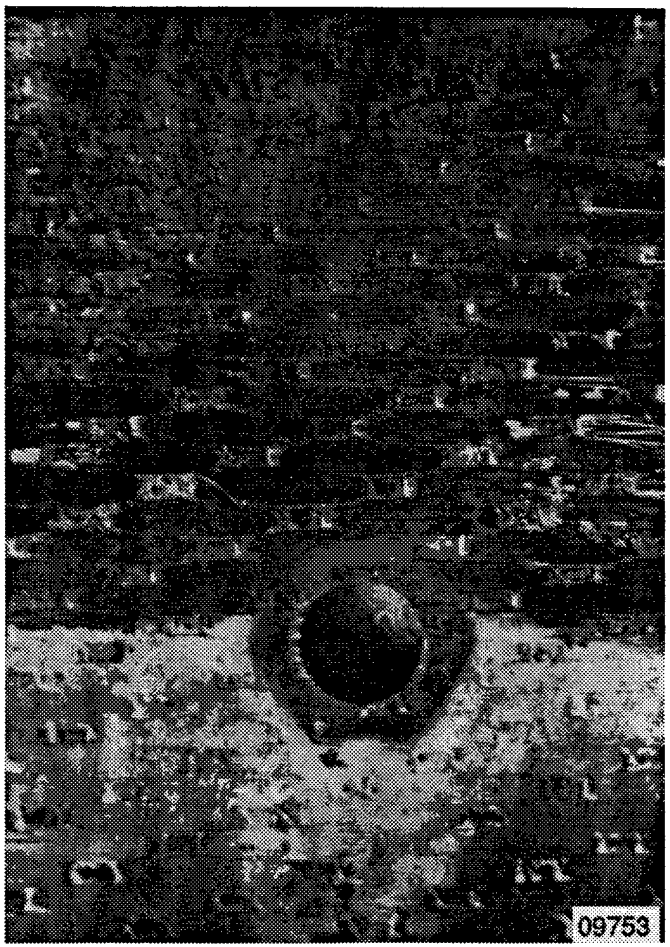


*Figure 10c. Close-up view of a Matrimid 5292 sample corroded 96 hr at 80°C*

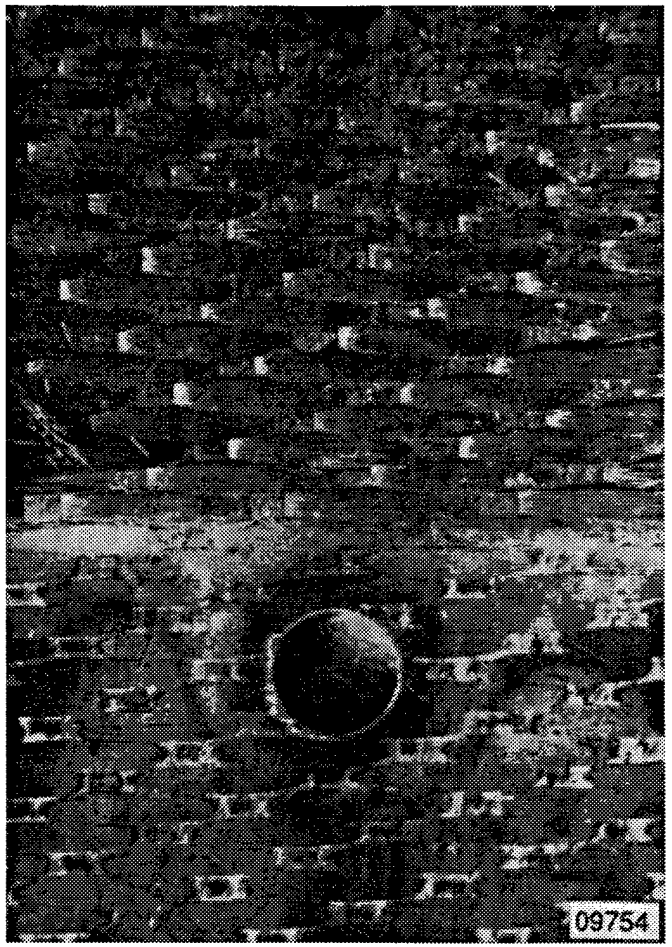


*Figure 10d. Close-up view of a Plenco 12505 modified sample corroded 96 hr at 80°C*

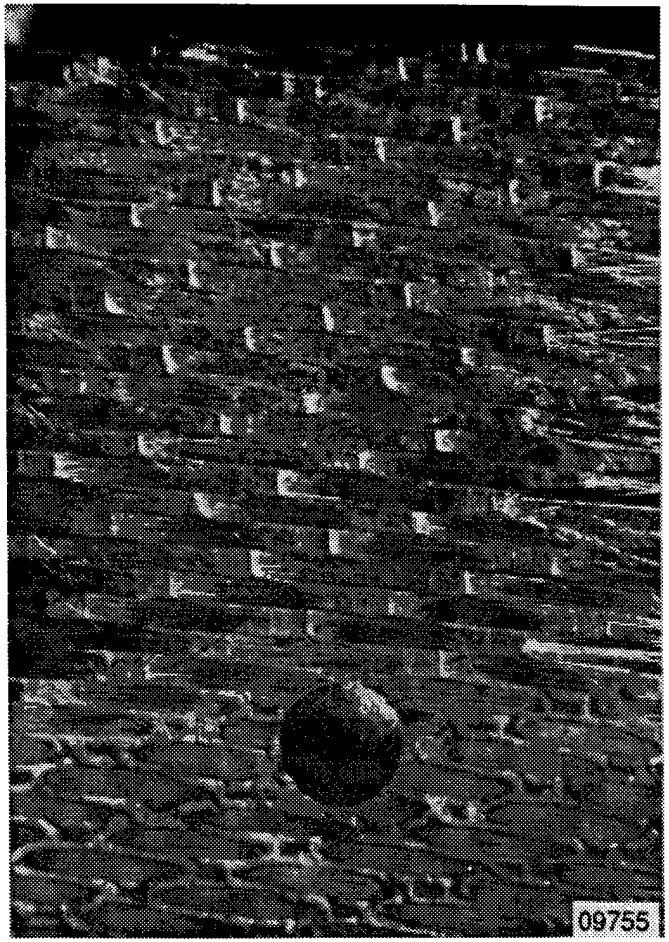


*Figure 10e. Close-up view of a Penacolite B-1A modified sample corroded 96 hr at 80°C*

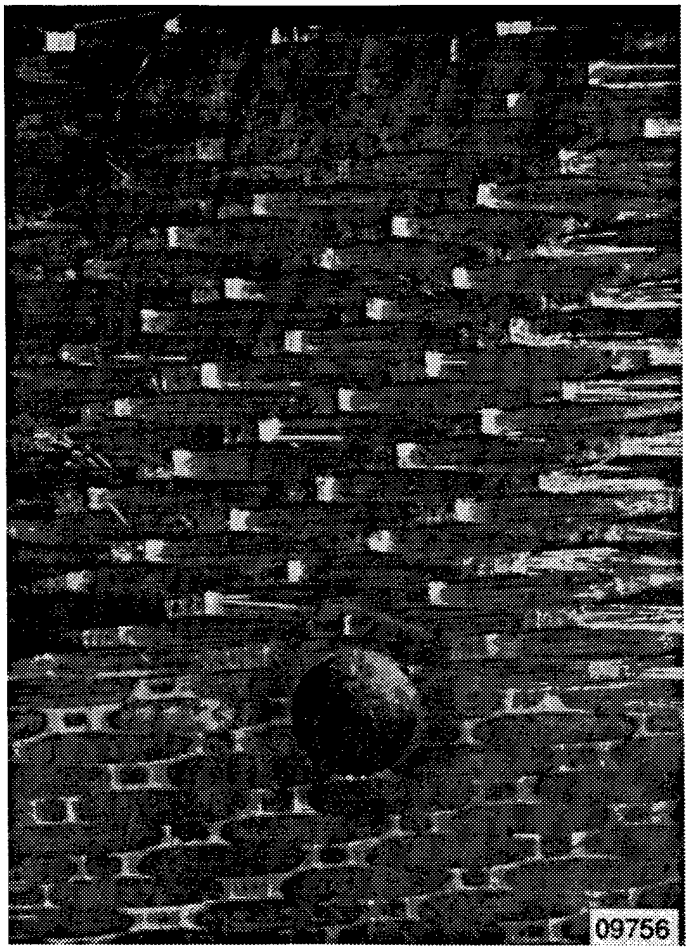


*Figure 10f. Close-up view of an epoxy coated fiber sample corroded 96 hr at 80°C*

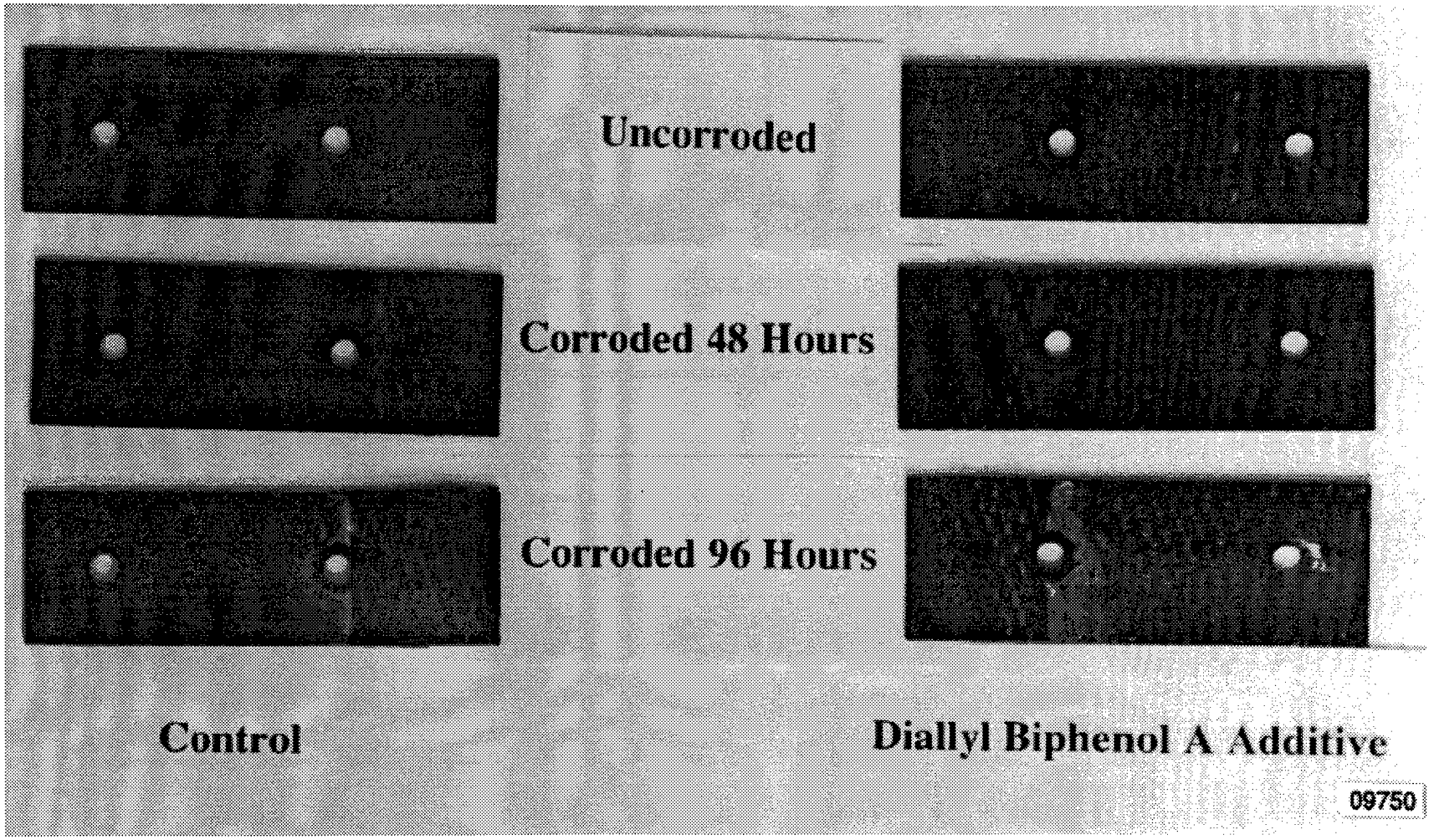


***Figure 11a. Photos of BMI control and Matrimid samples which were uncorroded, corroded for 48 hr, and corroded for 96 hr***

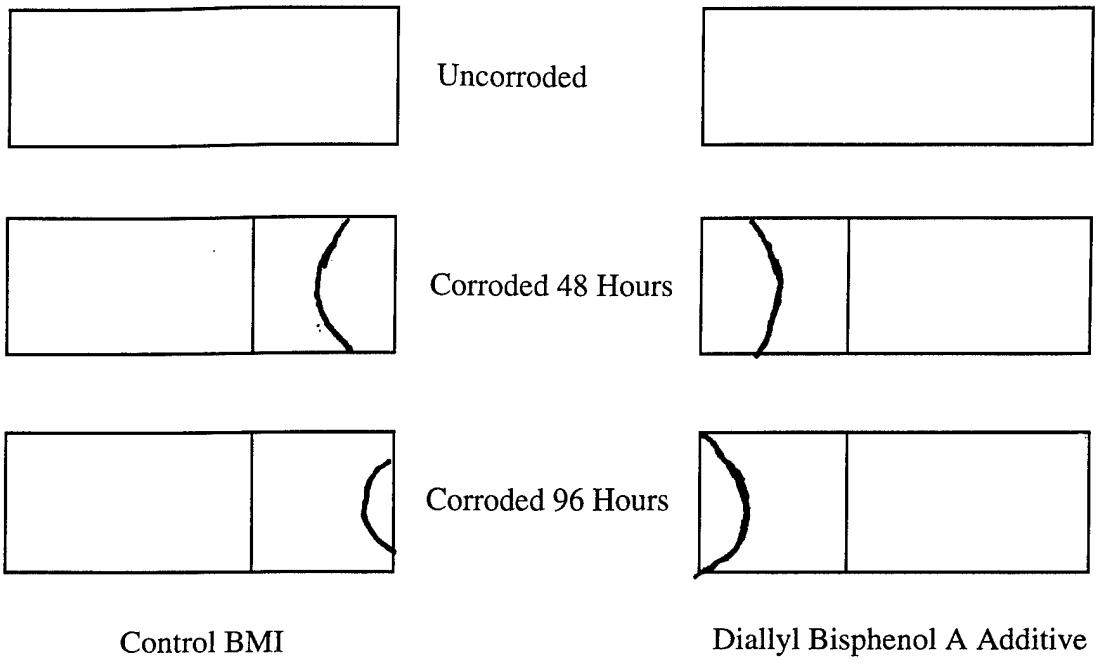


***Figure 11b. Illustration of the size of the corroded region for samples in Figure 11a***

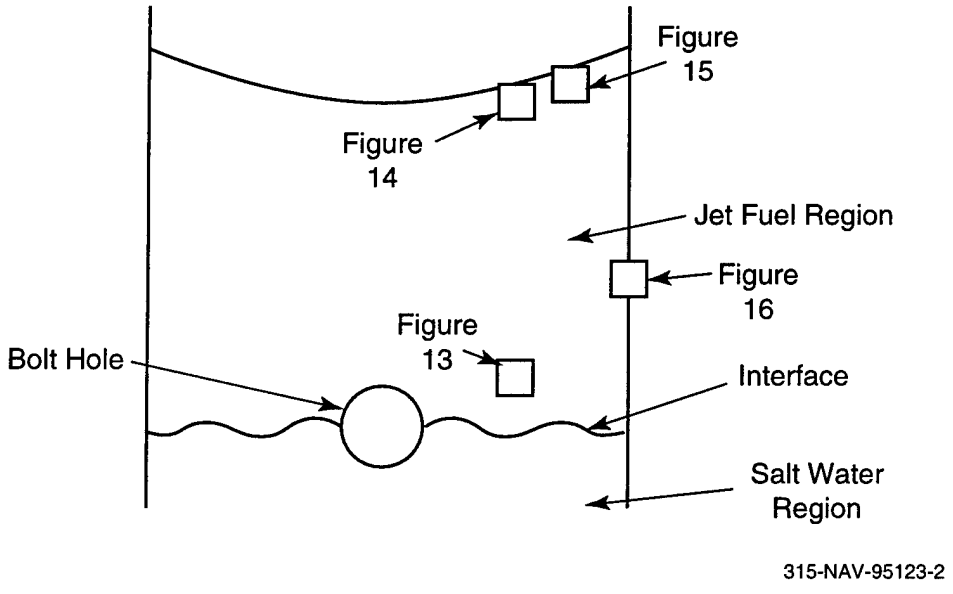


***Figure 12. Locations on samples from which optical micrographs were taken***

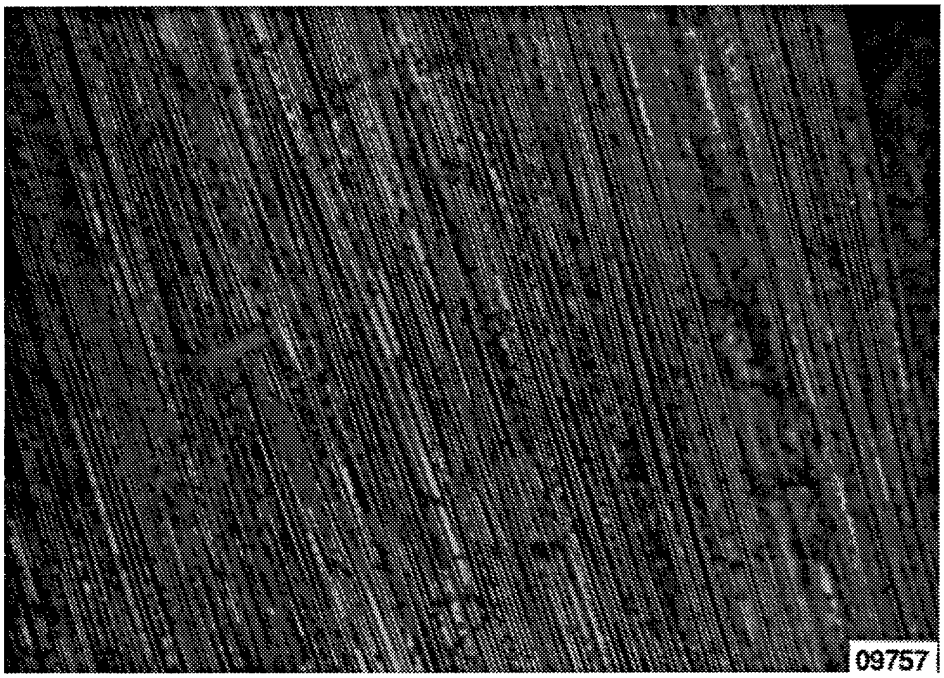


***Figure 13. Bare fibers in the center of the corrosion region in the Matrimid sample corroded for 48 hr***

A region of the 48 hr corroded control and Matrimid samples, taken closer to the saltwater-jet fuel interface, is shown in Figure 21. Here, transverse microcracks have broken the surface resin into smaller fragments, and some of these fragments have begun to flake off. A closer examination of this flaking process is shown in Figure 22. Figure 22a shows a region where both longitudinal and transverse microcracking has occurred. When viewed at a higher tilt angle and at higher magnification in Figures 22b and 22c, the surface resin is seen to be peeling away from the carbon fiber beneath it. This confirms that after microcracks initiate, corrosion progresses locally along the fiber-matrix interface. The debonded region is observed to curl away from the fiber surface, further exposing the fiber. This curling is probably a result of the residual tensile stresses in the resin, which also drives propagation of the microcracks.

Above the saltwater-jet fuel interface, bare fibers are seen, as in Figure 23. Only small fragments of resin remain in regions where the resin was locally thick, such as in the resin pockets where the fiber tow dives beneath the surface of the weave structure. A resin rich pocket is illustrated in Figure 24.

Conspicuously absent from any of the resin surfaces of the corroded samples are signs of extensive pitting or surface attack. The only surface features which are highly prominent are residues, such as salt or corrosion by-product, which were not removed during rinsing. Instead, it appears that most resin was removed by stress-corrosion induced microcracking and subsequent flaking of relatively large segments of material. This mechanism is illustrated in Figure 25. This resin removal exposed further carbon fiber, providing greater surface area for the cathodic reaction. Thus, it is likely that the exposure of more carbon fiber during corrosion causes an acceleration of the corrosion process.


*Figure 14a. A view of microcracking in a thick region of resin near the corrosion front of the Matrimid sample corroded for 48 hr*


*Figure 14b. A view of the uncorroded BMI control sample showing a region of the sample similar to that in Figure 14a*

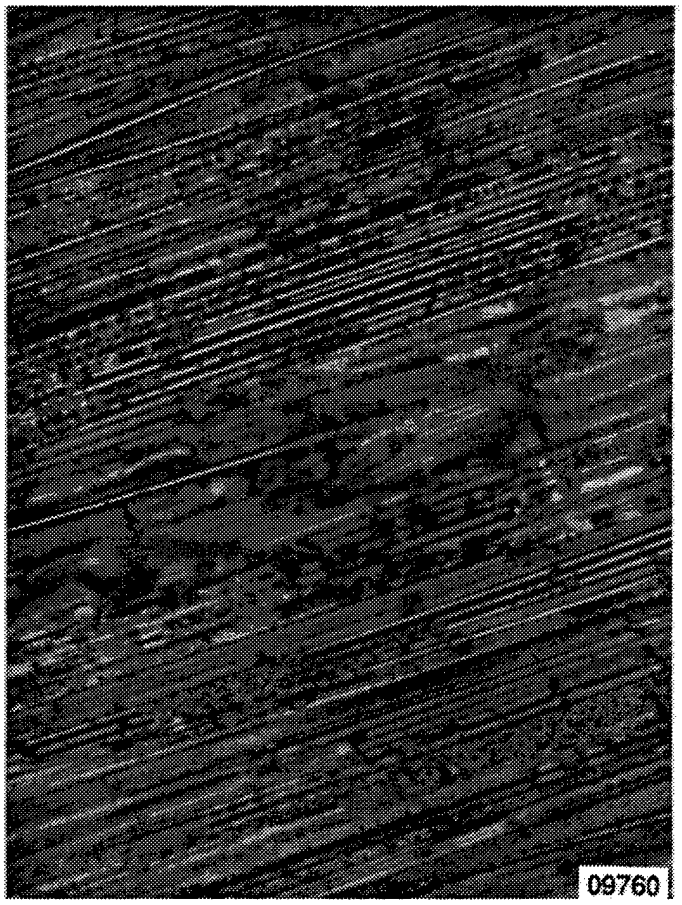


*Figure 15. Fragments of resin peeling away from the composite surface in the 48 hr corroded BMI control sample*

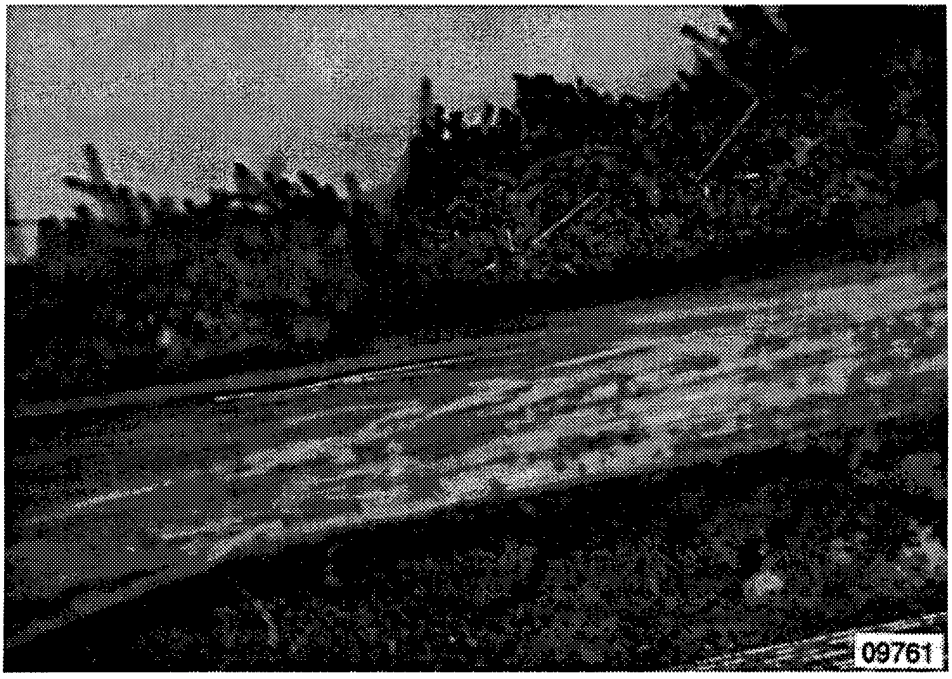


*Figure 16. An edge view of the BMI control sample corroded for 48 hr*

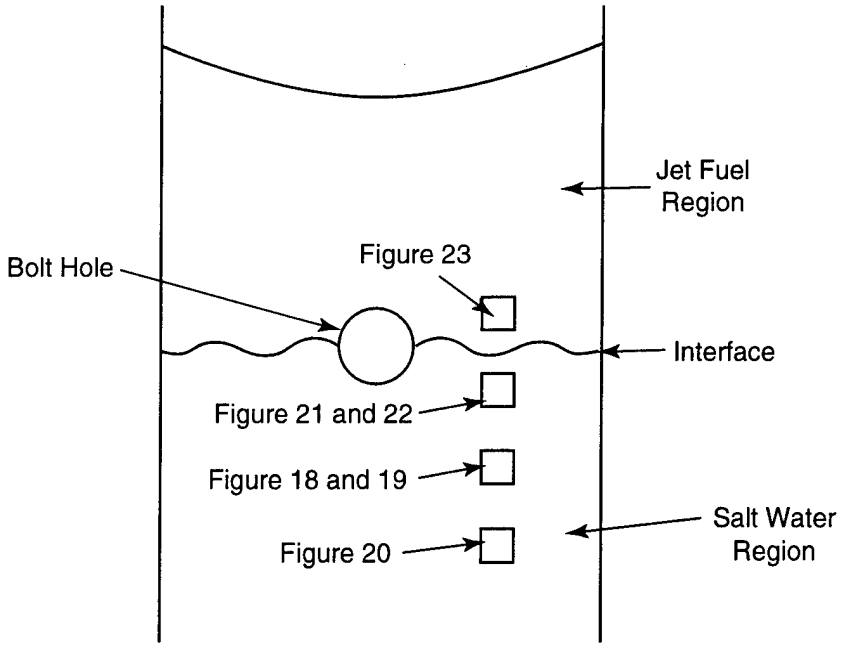


***Figure 17. Locations on samples from which SEM micrographs were taken***

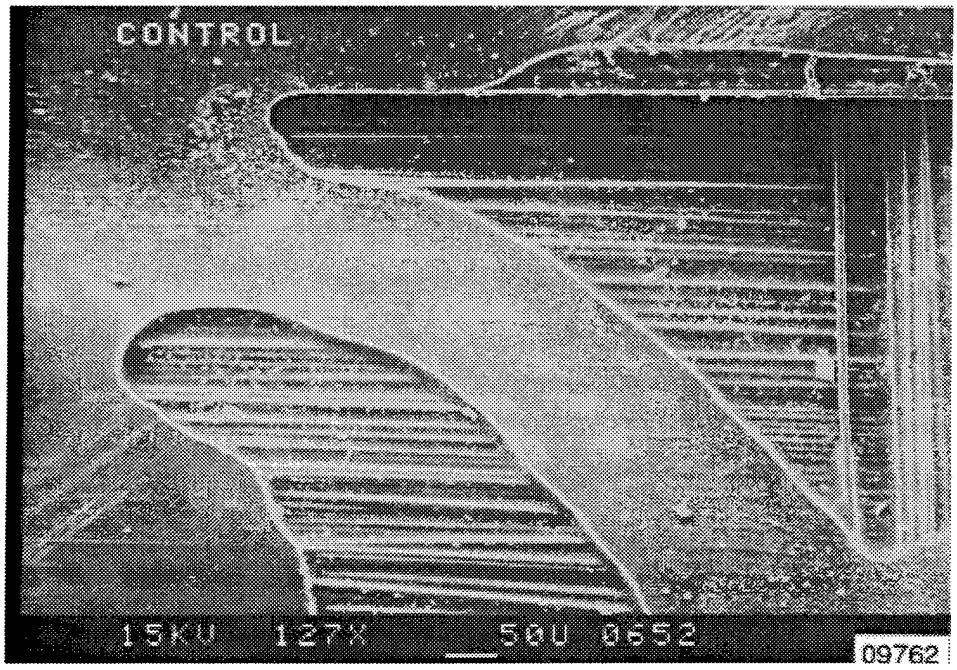


A) THE UNCORRODED CONTROL SAMPLE, TAKEN NEAR THE INTERSECTION OF WOVEN FIBER TOWS. EMBEDDED SURFACE FIBERS ARE SEEN IN TWO SMALL SURFACE VOIDS

***Figure 18. 130x views of BMI control and Matrimid samples which were uncorroded and corroded for 48 hr at 80°C***


B) THE CONTROL SAMPLE CORRODED FOR 48 HR, VIEWED IN A REGION WELL BELOW THE SALTWATER-JET FUEL INTERFACE. NOTE THE EXTENSIVE MICROCRACKING OF THE RESIN

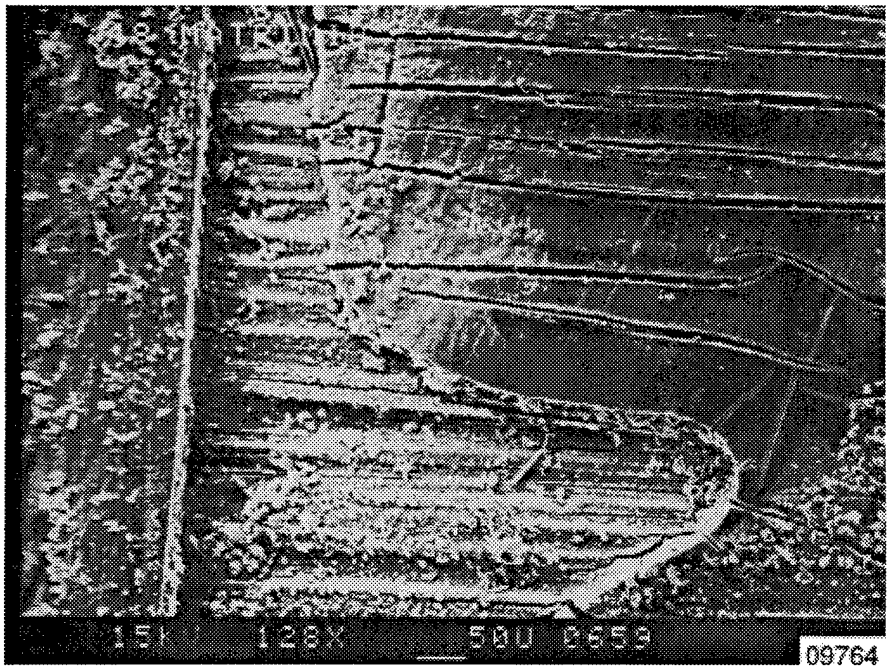


C) THE MATRIMID SAMPLE CORRODED FOR 48 HR, VIEWED IN A REGION WELL BELOW THE SALTWATER-JET FUEL INTERFACE. NOTE THE SURFACE VOID SIMILAR TO THAT IN FIGURE 18A, AS WELL AS THE EXTENSIVE MICROCRACKING OF THE RESIN

***Figure 18. 130x views of BMI control and Matrimid samples which were uncorroded and corroded for 48 hr at 80°C (continued)***

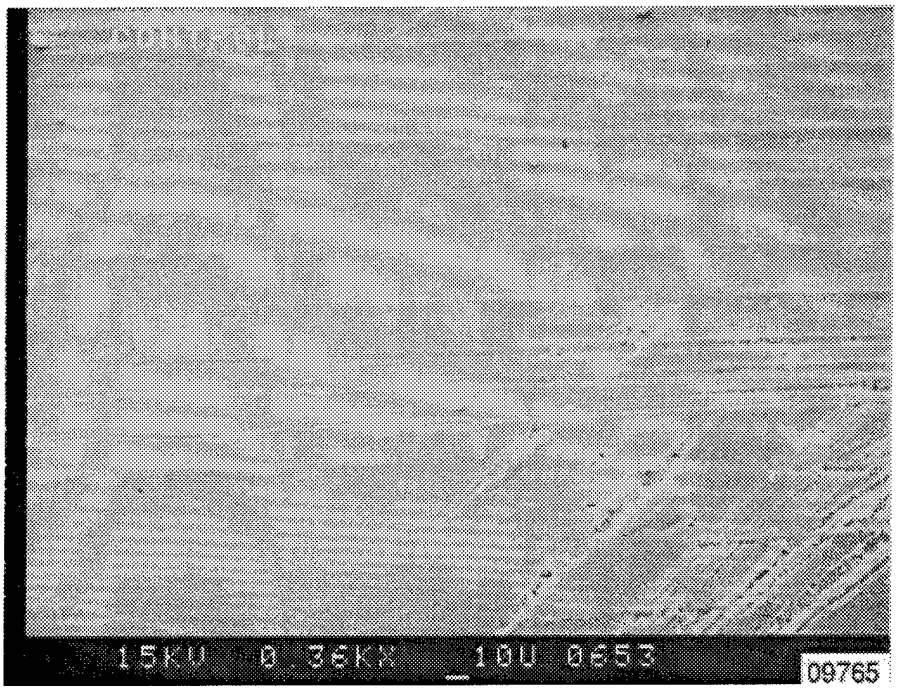


A) THE SURFACE OF THE UNCORRODED CONTROL SAMPLE. AN EXTENSIVE SURVEY OF THE SURFACE DID NOT ILLUMINATE ANY MICROCRACKS


B) THE CONTROL SAMPLE CORRODED FOR 48 HR, VIEWED IN A REGION WELL BELOW THE SALTWATER-JET FUEL INTERFACE. NOTE THE EXTENSIVE MICROCRACKING OF THE RESIN

***Figure 19. 360x views of BMI control and Matrimid samples which were uncorroded and corroded for 48 hr at 80°C***

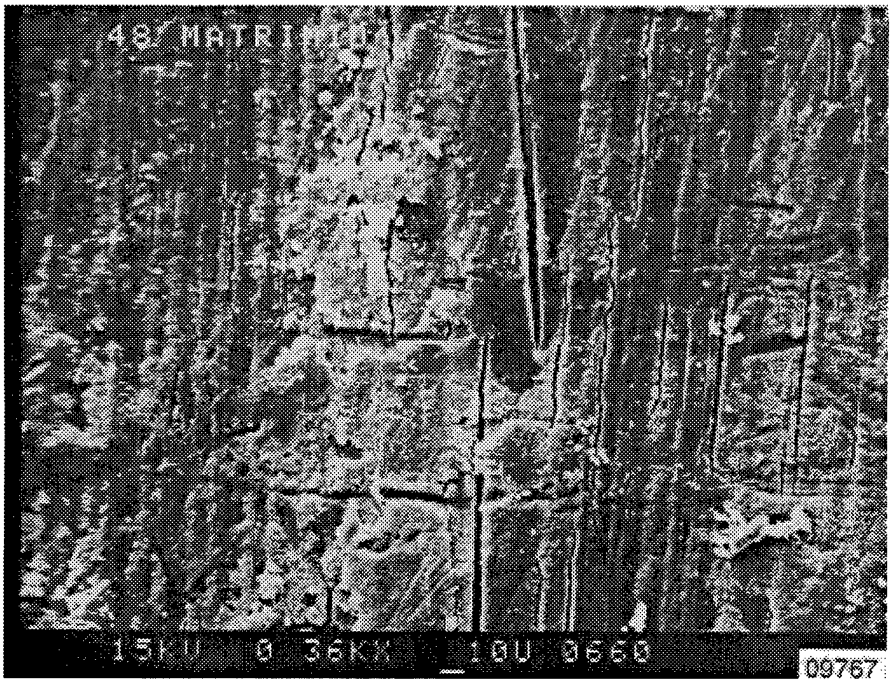


C) THE MATRIMID SAMPLE CORRODED FOR 48 HR, VIEWED IN A REGION WELL BELOW THE SALTWATER-JET FUEL INTERFACE. NOTE THE EXTENSIVE MICROCRACKING OF THE RESIN

***Figure 19. 360x views of BMI control and Matrimid samples which were uncorroded and corroded for 48 hr at 80°C (continued)***

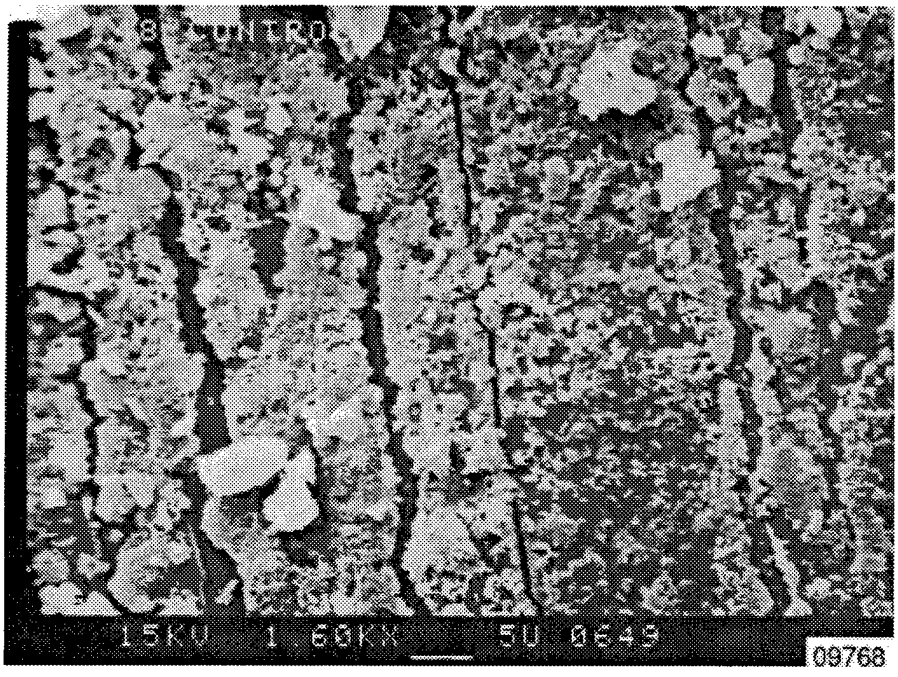


***Figure 20. Initiation zone of microcracks in a BMI control sample corroded for 48 hr***

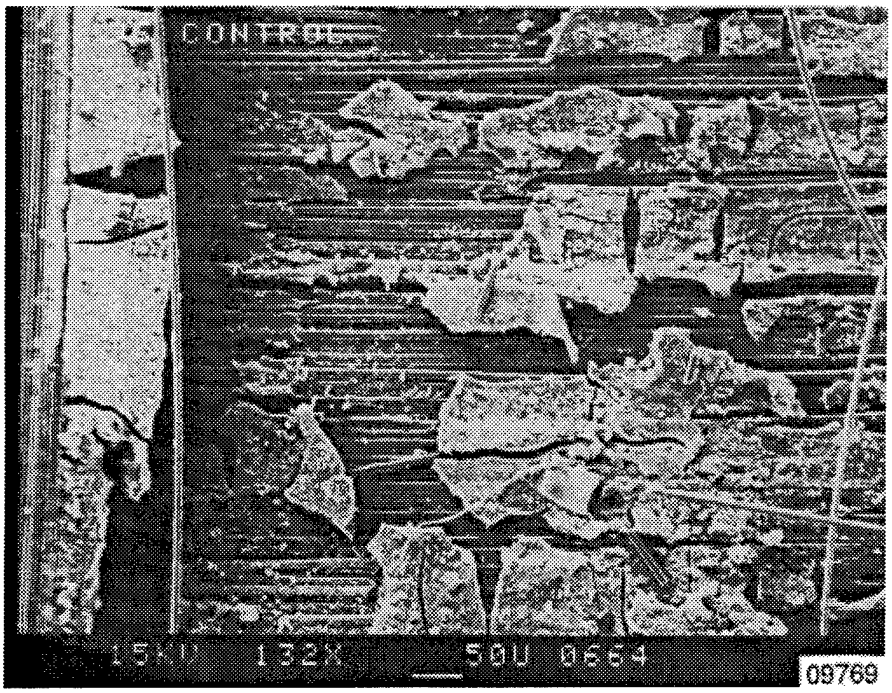


A) THE BMI CONTROL SAMPLE CORRODED FOR 48 HR, VIEWED IN A REGION JUST ABOVE THE SALTWATER-JET FUEL INTERFACE. NOTE THE TRANSVERSE MICROCRACKING AND FLAKING OF THE RESIN

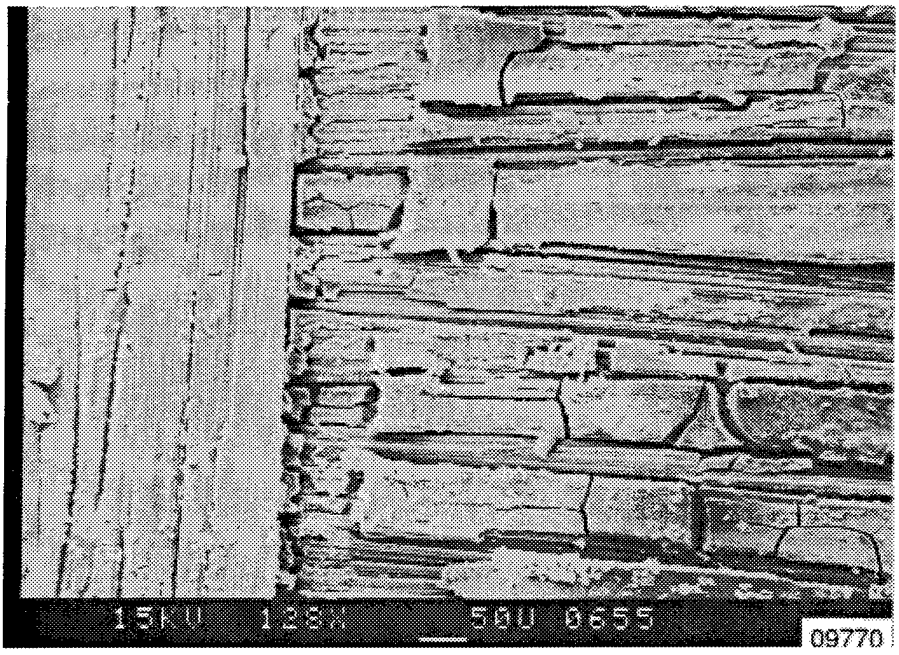


B) THE MATRIMID SAMPLE CORRODED FOR 48 HR, VIEWED IN A REGION JUST ABOVE THE SALTWATER-JET FUEL INTERFACE. NOTE THE TRANSVERSE MICROCRACKING AND FLAKING OF THE RESIN

***Figure 21. 130x views of BMI control and Matrimid samples which corroded for 48 hr at 80°C. This view is taken just below the saltwater-jet fuel interface***

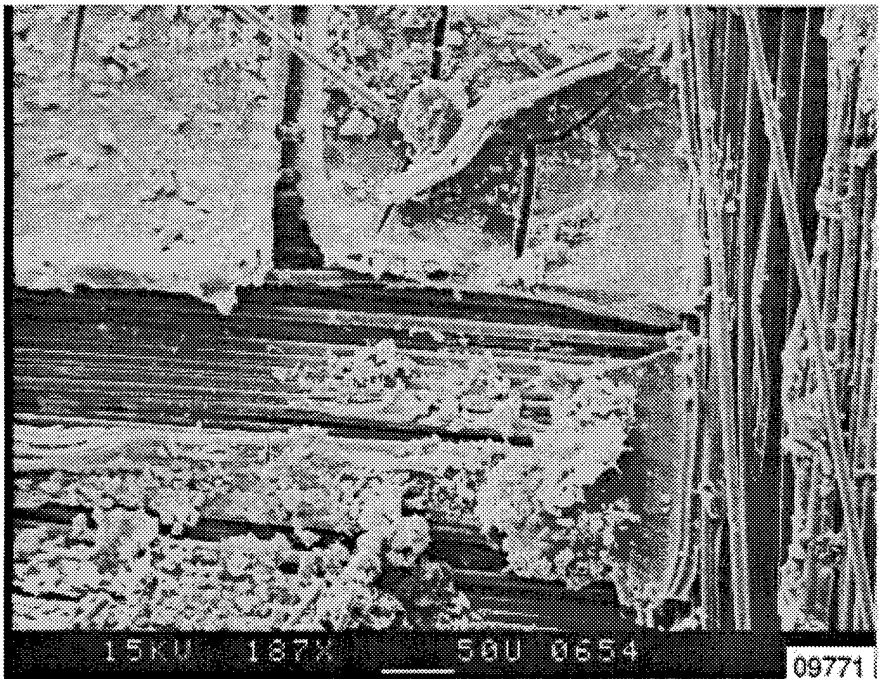


A) LOW MAGNIFICATION VIEW OF THE FLAKING AND PEELING INITIATION IN THE CENTER OF THE MICROGRAPH

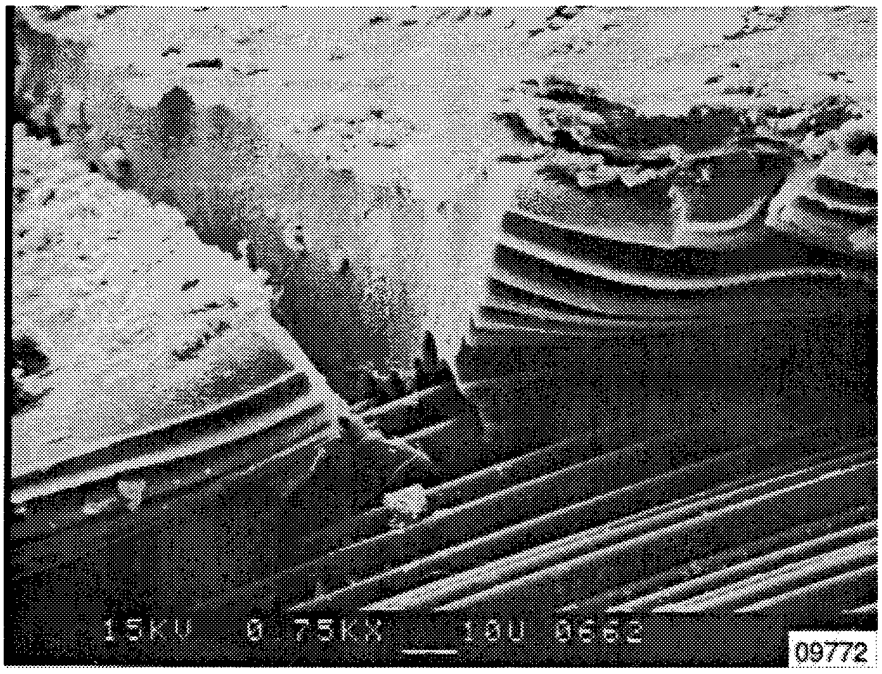


B) HIGHER MAGNIFICATION VIEW OF FIGURE 22A WITH TILT INCREASED TO 65 DEG

***Figure 22. Examination of the flaking process in the Matrimid sample corroded for 48 hr at 80°C***

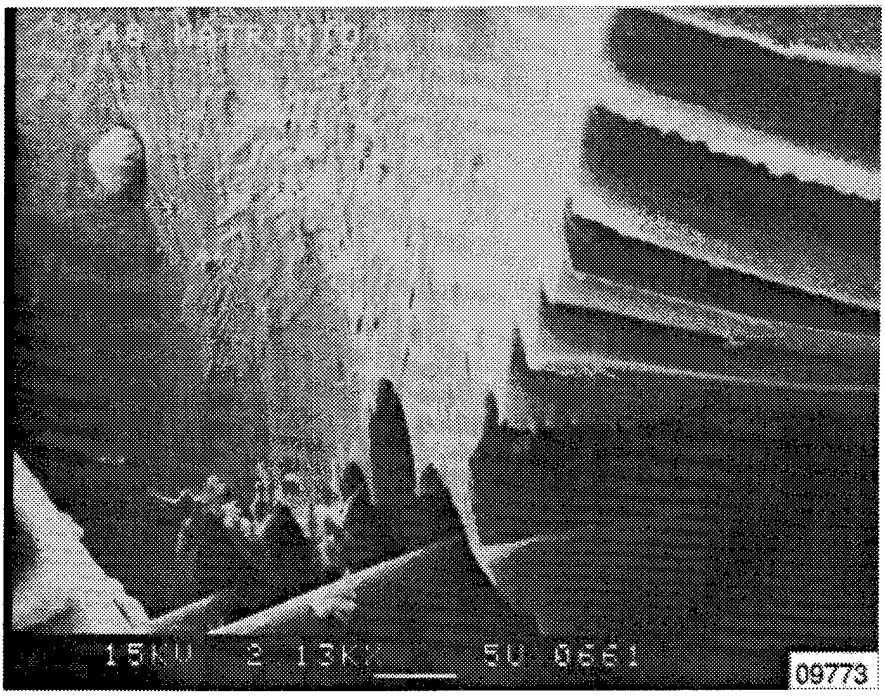


C) HIGHER MAGNIFICATION VIEW OF FIGURE 22B WITH TILT AT 65 DEG

***Figure 22. Examination of the flaking process in the Matrimid sample corroded for 48 hr at 80°C (continued)***

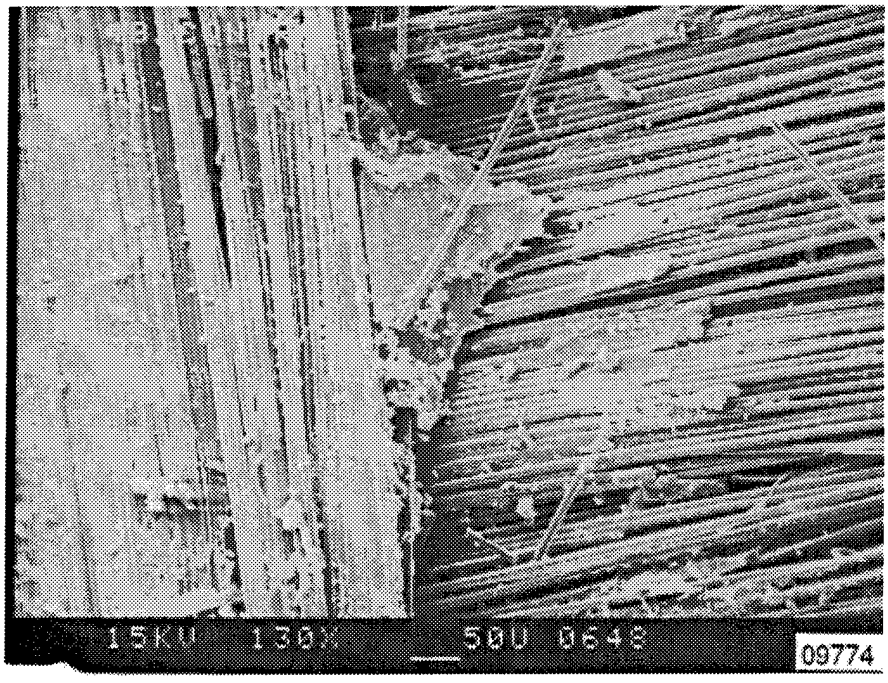


***Figure 23. A view of the 48 hr corroded BMI control sample taken above the saltwater-jet fuel interface***

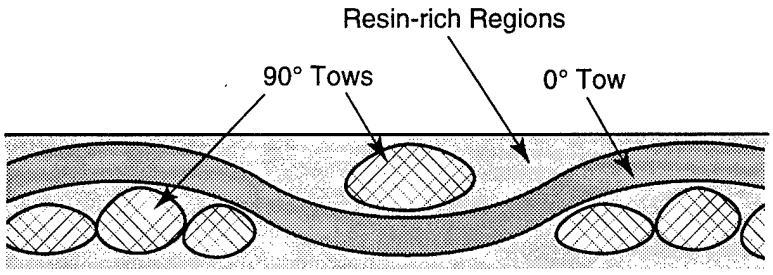


310-NAV-951233-3

***Figure 24. End section of composite showing resin-rich regions on surface***

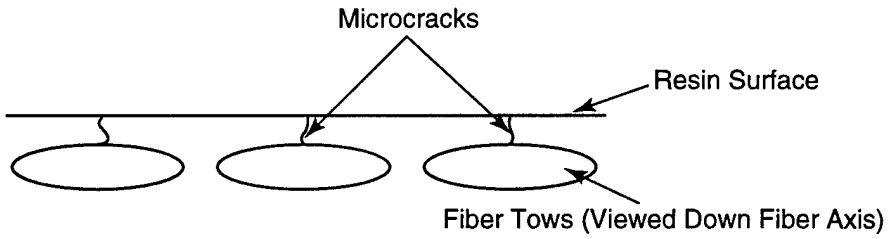


a) Microcracks Extend From Resin Surface To Fiber Tows

b) Microcracks Propogate Along Fiber-matrix Interface

c) Resin Fragments Flake Off, Exposing Fiber Surface

314-NAV-95123-1

***Figure 25. Mechanism of resin removal during corrosion***

It was with this mechanism in mind that we attempted to use an epoxy coating to insulate the fibers. Since the epoxy is resistant to galvanic corrosion in this system, it was hoped that it might remain as a coating on the fiber surface and thereby prevent propagation of the corrosion front along the fiber-matrix interface beneath the surface of the resin. This would prevent or reduce flaking of the large fragments of uncorroded resin, which in turn would reduce the exposed fiber area, thereby slowing the propagation of the corrosion front. However, results from the epoxy coated fiber samples indicate that corrosion was not retarded significantly in this system. Since the epoxy coating was probably only a fraction of a micron thick on average, it is difficult to determine exactly why it failed to perform as had been hoped.

The mechanisms by which microcracks are initiated during corrosion are not entirely clear. It is likely that microcracks initiate either at the fiber ends, where the production of hydroxyl ions is most concentrated, or in the resin on the composite surface. In either case, it is likely

that both residual tensile stresses in the resin (due to matrix-fiber CTE mismatch) and the presence of hydroxyl ions are necessary for corrosion to occur.

### 3.2.6 Bearing Strength Testing of Corroded Test Coupons

The bolt bearing strength of corroded and uncorroded samples was measured. Samples were cut as shown in Figure 6c prior to testing. Testing was performed on an Instron servo-hydraulic testing machine. The loading rate was 0.05 in./min. Samples were loaded until the first load drop or substantial change in slope was observed in the load-deflection plot. A representative plot for an uncorroded BMI control sample corroded 96 hr is shown in Figure 26.

A summary of the bearing strength tests is shown in Table 8. The same data is plotted in Figure 27. Since five data points were obtained for nearly all sample groups, the standard deviation is approximately equal to the 95 percent confidence interval.

A summary of the retention of bearing strength (relative to uncorroded strength) is shown in Table 9. In Table 9, the retention values are based on the average strengths of the corroded and uncorroded samples. The range of retention was calculated to provide an estimate of the significance of the retention data. The lower limit (L) of the retention range was calculated as:

$$L = (B_c - S_c) / (B_u + S_u)$$

and the upper limit (U) was calculated as:

$$U = (B_c + S_c) / (B_u - S_u)$$

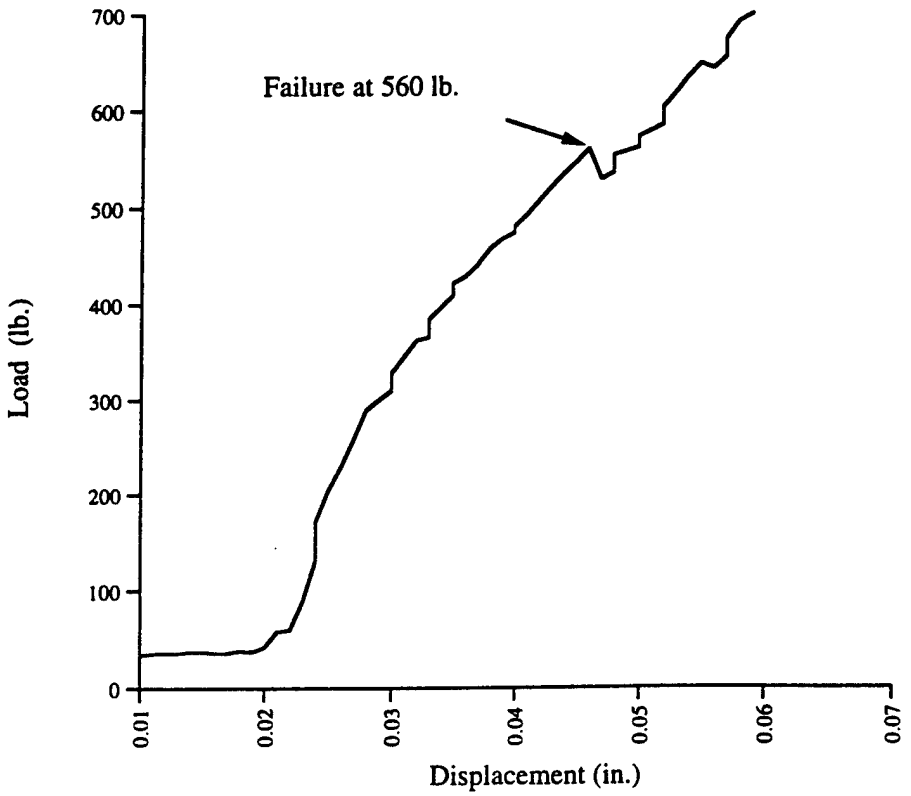


***Figure 26. Load-deflection plot for a control sample corroded 96 hr at 80°C***

*Table 8. Bolt bearing strength results for samples corroded at 80°C*

| | Uncorroded | | Corroded 48 hr | | Corroded 96 hr | |
|---|---|---|---|---|---|---|
| | Strength (ksi) | Standard Deviation | Strength (ksi) | Standard Deviation | Strength (ksi) | Standard Deviation |
| BMI Control | 812 | (47) | 718 | (93) | 536 | (84) |
| Matrimid 5292 | 819 | (101) | 770 | (5) | 621 | (109) |
| Plenco 12505 | 940 | (16) | NA | NA | 646 | (79) |
| Penacolite B-1A | 741 | (94) | NA | NA | 564 | (186) |
| Epoxy Coated Fibers | 773 | (81) | NA | NA | 714 | (127) |

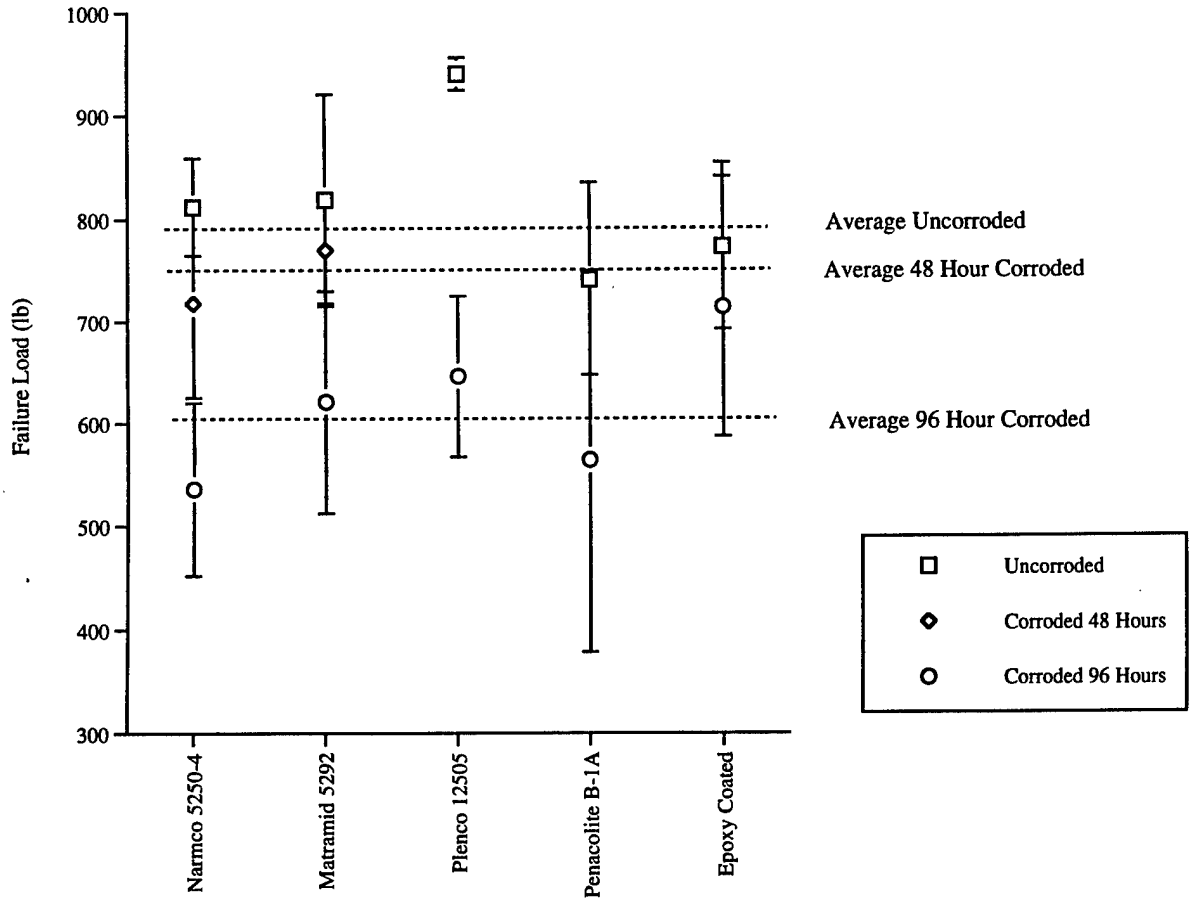


*Figure 27. Bolt bearing strength results for samples corroded at 80°C*

where:

$B_c$ was the bearing strength of the corroded samples
$S_c$ was the standard deviation of the corroded samples
$B_u$ was the bearing strength of the uncorroded samples
and $S_u$ was the standard deviation of the uncorroded samples

***Table 9. Percent retention of bolt bearing strength for samples corroded at 80°C***

| | Corroded 48 hr | | Corroded 96 hr | |
|---|---|---|---|---|
| | Retention | Range | Retention | Range |
| BMI Control | 88% | 73 to 106% | 66% | 53 to 81% |
| Matrimid 5292 | 94% | 78 to 115% | 76% | 56 to 102% |
| Plenco 12505 | NA | NA | 69% | 59 to 78% |
| Penacolite B-1A | NA | NA | 76% | 45 to 116% |
| Epoxy Coated Fibers | NA | NA | 92% | 69 to 121% |

The samples corroded for 48 hr show only a moderate, statistically insignificant loss in bearing strength, despite the presence of significant visible corrosion. The samples corroded for 96 hr show a significant reduction in bearing strength. However, the improvements in bearing strength for the modified samples are not statistically significant. In the case of the epoxy coated fiber samples, which showed the greatest improvement in bearing strength, the visible corrosion appeared no different from that of the control. We expect that the difference in strength retention for this sample is due to the greater thickness (lower fiber volume fraction) of these samples; if the depth of corrosion is similar to that of the control samples and the sample thickness is greater, then the *relative* depth of the corrosion is less. Our conclusion is that the corrosion resistance of the modified systems was not improved significantly over that of the control.

### 3.2.7 Summary of Experimental Findings and Conclusions

While the corrosion resistance of BMI matrix composites was not improved using the approaches taken in this research, a greater understanding of the mechanisms by which corrosion occurs in these systems was achieved. The following is summary of the findings of this research.

*Objective: Establish mechanism of hydroxyl attack of BMI*

- Potential upper and lower bounds to the rate of corrosion were measured. The absorption of moisture by the BMI resin composite obscured the accuracy of the results.

- The mechanism by which corrosion progresses was determined to be stress corrosion cracking. Internal stresses in the BMI matrix, due to a CTE mismatch between the fiber and matrix, drive the microcracking of the resin in the presence of hydroxyl groups. After the microcracks have broken the surface layer of resin into fragments, corrosion progresses along the fiber-matrix interface beneath the resin surface. This causes peeling of the resin away from the fiber surface, eventually causing the fragments to flake off. This in turn exposes more bare fiber, which increases the rate of hydroxyl group generation, which in turn leads to an acceleration of the corrosion process.

*Objective: Select modifications for imide based resins*

- Six hydroxyl scavengers were identified and obtained.

- Testing of BMI solubility, modified resin Tg (via DSC), and clear casting flexural strength was used to screen the scavengers. Three scavengers were selected for composite fabrication and corrosion studies.

*Objective: Fabricate modified graphite fiber reinforced BMI test coupons*

- Five composite panels were fabricated, including one BMI control panel, three modified BMI panels, and one epoxy coated fiber panel.

*Objective: Evaluate means to prevent corrosive attack*

- Modification of the BMI matrix with hydroxyl scavengers was accomplished but did not lead to improving the resistance of the composite to galvanic corrosion.

- Epoxy coated fibers were used in an attempt to defeat the mechanism by which corrosion propagates. This attempt, which was based on our corrosion mechanism findings, did not improve corrosion resistance. However, it is possible that fibers coated with more epoxy, or fibers coated with a different material (such as a high temperature thermoplastic), may reduce or prevent corrosion.

*Objective: Test bearing strength of modified test coupons before and after exposure, with and without modified resin*

- The bearing strength of the BMI control samples was not reduced significantly after 48 hr of corrosion at 80°C. Hence, any improvements from modifying the resin would not be detected at this level of corrosion.

- After 96 hr of corrosion at 80°C, the bearing strength of the BMI control samples was reduced 66 percent. The modified samples did not show a statistically significant improvement in bearing strength over the control. While the epoxy coated fiber sample did exhibit a higher level of strength retention, this was attributed to its greater thickness and lower volume fraction fiber, and not to any improvement in corrosion resistance.

# 4. PHASE I ACCOMPLISHMENTS AND IMPLICATIONS FOR PHASE II

## 4.1 Phase I Accomplishments

This Phase I effort verified mechanisms of imide composite degradation which had been speculated upon but had not been verified previously. This understanding can be used to more effectively approach the problem of imide degradation in the future. This research also illustrated the limitations of the use of hydroxyl scavengers as a means of limiting or preventing galvanic attack. The research proposed fiber coating as a potential solution to this problem. While the preliminary attempt using epoxy coatings in this study did not succeed, other coatings might be identified which could be effective in reducing corrosion. A detailed accounting of our Phase I accomplishments was presented in subsection 3.2.

## 4.2 Implications for Phase II

While we remain encouraged by the potential offered by fiber coatings, further research will need to be performed before the production of a fiber coating to retard the corrosion mechanism. This effort would consist of the following tasks:

- Further examine the initiation of corrosion-induced microcracking: Samples would be corroded for various lengths of time to capture the initiation and growth of both microcracks and the corrosion front. Optical and SEM examination of these samples would be used to further elucidate the corrosion mechanisms.

- Reduce the CTE mismatch via modification of the cure schedule: Since the residual stresses are largely governed by the temperature at which the resin gels, modification of the cure schedule to lower the gelation temperature could reduce the driving force for microcrack generation.

- Identify candidate materials for fiber coating: Previous research (8) evaluated four thermoplastic coatings to improve the microcracking resistance and thermo-oxidative stability of PMR-15 matrix composites. One coating material provided promising results. The results of this study can provide guidelines for the selection of further coating materials.

- Identify appropriate coating thicknesses and procedures: The coating must be applied in a way to prevent fiber tow agglomeration while ensuring adequate coating thickness. Coating studies would be performed to evaluate coating techniques and coating thicknesses.

- Evaluate the effectiveness of coatings: Composite samples would be fabricated using the coated fiber materials. Samples would be corroded for various times to determine the corrosion resistance of the coated fiber composites. SEM and optical microscopy would be used to compare corrosion mechanisms to those of the uncoated fiber control samples. Bearing strength would be evaluated on promising materials.

# 5. REFERENCES


1. R.C. Cochran, R.E. Trabocco, J. Boodey, J. Thompson, and T.M. Donnellan, 36th International SAMPE Symposium, April 15-18, 1991, p. 1273.
2. M.C. Faudree, 36th International SAMPE Symposium, April 15-18, 1991, p. 1288.
3. D.R. Askins, AFWAL-TR-83-4125, Dec. 1983.
4. C.J. Wolf and R.S. Soloman, SAMPE Jan/Feb 1984, p. 16.
5. Military Specification TTS-735, Type VII.
6. Military Specification MIL-C-27725.
7. W.H. Ailor, *Handbook on Corrosion Testing and Evaluation*, John Wiley and Sons, Inc., New York, 1971.
8. S.D. Jenkins, G.T. Emmerson, P.T. McGrail, and R.M. Robinson, *Journal of Adhesion*, V. 45, Issue 1-4, 1994, p. 15.